Journal of Materials Chemistry C

ROYAL SOCIETY OF CHEMISTRY

PAPER

View Article Online
View Journal | View Issue

Cite this: J. Mater. Chem. C, 2024, 12, 19643

Effect of counterion tether length on stability, work function and application of a self-compensated, hole-doped triarylamine-*alt*-fluorene model polymer†

Qi-Mian Koh,[a] Kevin Christopher Boellaard,[a] Yu Wang,[a] Cindy G. Tang,[b] Qiu-Jing Seah,[a] Peter. K. H. Ho,[b] Rui-Qi Png *[b] and Lay-Lay Chua *[ab]

Self-compensated, hole-doped polymers with ultrahigh workfunction can provide ohmic hole contacts even for deep-ionization-energy semiconductors. The self-compensation is usually imposed by an anion tethered to a flexible $-(CH_2)_n-$ chain, but the effect of tether length n is unknown. Here, using the mTFF triarylamine–fluorene as a model semiconductor, we have designed, synthesized and characterized a family of mTFF-CnSISC_2F_5 polymers, where C_2F_5SIS is the pentafluoroethanesulfonylimidosulfonyl anion, tethered to a Cn alkylene chain that is systematically varied between C2 and C6 in length. Solution doping yields self-compensated films with a work function of *ca.* 5.75 eV, which is *ca.* 0.15 eV higher than that obtained by film doping and higher than that of the corresponding hole-doped mTFF films counterbalanced by SbF_6^- anions. We attribute the higher work function to a frustrated packing of the counteranions about the holes. The ultrahigh work function is consistent with electroabsorption measurements and the ability of the films to inject holes into PFOP, a model deep-ionization-energy semiconductor, without bias pre-conditioning. While the tether length only weakly influences the work function, it strongly influences hygroscopicity, processability, and thermal stability of the hole-doped polymers. OPLS4 molecular dynamics simulations suggest that short tether lengths (C2 and C3) result in interchain charge compensation, but medium and long tether lengths (C4 and C6) result in mixed interchain/intrachain charge compensation. Overall, the C3 tether provides the best thermal and ambient stability. These results reveal new aspects regarding the role of tether length in self-compensated, charge-doped polymers.

Received 30th May 2024,
Accepted 5th September 2024

DOI: 10.1039/d4tc02228a

rsc.li/materials-c

Introduction

Optimization of the performance of organic semiconductor (OSC) devices, such as organic light-emitting diodes and solar cells, requires tailoring the work function of charge injection or collection layers. This is significantly aided by the recent development of self-compensated (SC) charge-doped polymers of both charge signs, where the free carriers on the polymer backbone are counterbalanced by tethered ions.[1,2] This self-compensation stabilizes the doping level, preventing dopant migration and thus enabling precise control of the doping profile in the device.[1,2] Furthermore, these materials offer tunable work functions spanning an ultrawide range (2.5 to 6.0 eV) through the span of ionization energies (I_E) and electron affinities (E_A) available by chemical design, further fine-tuned through the local Madelung potential effect by counterion and spectator-ion selection. This immense flexibility contrasts with traditional "self-doped" polymers that are limited to materials with low I_E for self-hole-doping, or high E_A for self-electron-doping.[3–6] The versatility of SC polymers is associated with separation of the charge-doping and charge-compensation processes. The polymer is doped by electron transfer with strong oxidants or reductants, and then compensated by association with tethered counterions by elimination of the dopant by-product. This approach has enabled the fabrication of high-performance solution-processed devices across various semiconductors,[7,8] including blue thermally activated delayed fluorescence light-emitting diodes,[9–11] perovskites,[12] and quantum dots.[13]

Using hole-doped triarylamine-*alt*-fluorene (TAF) copolymers as model systems,[14] the influence of various factors on the properties of SC polymers has been investigated.[1,15,16]

[a] Department of Chemistry, National University of Singapore, Lower Kent Ridge Road, Singapore, S117552, Singapore. E-mail: chmcll@nus.edu.sg
[b] Department of Physics, National University of Singapore, Lower Kent Ridge Road, Singapore, S117550, Singapore. E-mail: phypngrq@nus.edu.sg

† Electronic supplementary information (ESI) available. See DOI: https://doi.org/10.1039/d4tc02228a

These factors include the counteranion (*e.g.*, trifluoromethanesulfonylimidosulfonyl (CF_3SIS) *vs.* pentafluoroethanesulfonylimidosulfonyl (C_2F_5SIS)) and spectator cation (*e.g.*, Li^+ *vs.* Cs^+). Larger counteranions lead to weaker coulombic attraction of the hole carriers but stronger ion surface layering, which raises work function, while smaller spectator cations lead to stronger coulombic repulsion of the hole carriers, which also raises work function.[1,15,16] However, one critical aspect remains unexplored: the impact of length of the $-(CH_2)_n-$ flexible chain that tethers the counterion to the polymer backbone. We expect that short tethers would lead to interchain charge compensation, where the carrier on the polymer backbone is charge-balanced primarily by a counterion tethered to the adjacent polymer backbone, while long tethers would lead to mixed interchain/intrachain charge compensation, where the carrier is charge-balanced by a counterion tethered to the same or adjacent polymer backbone. This may affect ion cluster morphology and associated properties in non-trivial ways. Moreover, increasing the value of n increases the hydrophobic volume of the polymer and dilutes the semiconductor core fraction, which may also have unexpected effects.

In this work, we elucidate some of these effects, demonstrating that the tether length influences not only hygroscopicity and processability, but also stability of the SC hole-doped state. We studied poly[9,9-bis(ω-pentafluoroethanesulfonylimidosulfonylalkyl)fluorene-2,7-diyl-*alt*-1,4-phenylene-*N*-(*m*-trifluoromethylphenyl)imino-1,4-phenylene] with different tether lengths, denoted mTFF-C*n*SISC_2F_5, where n = 2, 3, 4 and 6, with sodium as the spectator cation. The spectator cation, together with doped hole if any, provides charge balance to the tethered anion. As a member of TAF polymers, mTFF exhibits non-dispersive and well-resolved frontier π-electron bands,[14] with relatively well-characterised ion clusters and surface layering behaviors,[15,16] and relatively well-understood electronic transition and transport properties.[17] Therefore, mTFF provides an excellent model to investigate the effects of tether length here. Our selection of C_2F_5SIS as the anion is driven by its stability[18] and low hygroscopicity.[19] Our selection of Na^+ as the spectator cation is driven by its favourable effect on work function[15] and processability.[16]

Results and discussion

Synthesis

The mTFF-C*n*SISC_2F_5 polymers were synthesized by microwave Suzuki coupling of the 9,9-bis(ω-pentafluoroethanesulfonylimidosulfonylalkyl)-2,7-dibromofluorene (diBr-FC*n*SISC_2F_5) monomer and the 4,4′-*N*-(*m*-trifluoromethylphenyl)iminobis-(phenylboronic acid pinacol ester) (mTF-diEs) monomer to give the respective polymers following the procedure reported in Tang *et al.*[1] and Ang *et al.*[16] Fig. 1 shows the generic chemical structure of the polymers.

Attaching the C_2F_5SIS anion to the fluorene moiety requires bespoke approaches for each tether length. For propyl and butyl tethers, syntheses of diBr-FC3SO_3Na and diBr-FC4SO_3Na were achieved by base-promoted 9-deprotonation of 2,7-dibromofluorene, followed by nucleophilic attack by the fluorene anion on the electrophilic carbon adjacent to the oxygen atom of commercially available sultones, *i.e.* 1,3-propanesultone and 1,4-butanesultone, to give diBr-FC3SO_3Na and diBr-FC4SO_3Na, respectively (Scheme 1a). However, β-sultone is unstable,[20] while 1,6-sultone is not commercially available. Hence, the syntheses of C2 and C6 tethered anions were achieved by different pathways. For **diBr-FC6SO_3Na**, the fluorene anion was reacted with 1,6-dibromohexane to give 9,9′-bis(bromohexyl)-2,7-dibromofluorene, and the tethered bromine then converted to iodine *via* Finkelstein reaction to provide a better leaving group for nucleophilic substitution reaction with sodium metabisulfite (Scheme 1b). This reaction could not be used for diBr-FC2SO_3Na due to facile competitive deprotonation of 1,2-dibromoethane to bromoethene. Instead, the monomer was synthesized by nucleophilic substitution on methyl bromoacetate by the fluorene anion, followed by reduction to the hydroxyethyl moiety,[21] substitution with iodide, then nucleophilic displacement with thiourea to yield isothiouronium, followed by acidification to cleave to hydrosulfide, and oxidation of the resultant diBr-FC2SH by performic acid to **diBr-FC2SO_3H** (Scheme 1c). This reaction is adapted from the synthesis of amino alkyl sulfonic acids.[22]

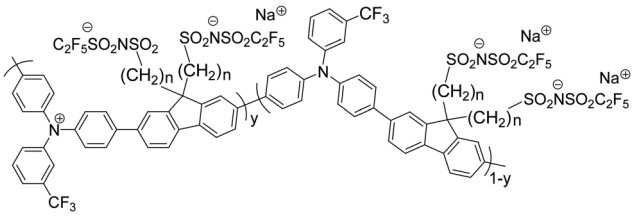

Fig. 1 Chemical structure of the self-compensated, hole-doped mTFF-C*n*SISC_2F_5 polymer. n denotes the number of CH_2 methylene units in the side-chain spacer (2, 3, 4 or 6). y denotes the doping level, in fraction of hole per repeat unit, where 0 represents the undoped polymer and 1 represents the fully hole-doped polymer.

In general, the ω-sulfonic acid monomers were subsequently converted to the corresponding C_2F_5SIS-tethered monomers, and polymerized with the **diEs-mTFF** monomer to give the mTFF-C*n*SISC_2F_5 polymers (see Experimental). Elemental analyses of the polymers gave satisfactory results (elemental ratio, ±5 atom%). The number-average molar masses by gel permeation chromatography were determined to be 26, 23, 14 and 19 kDa for n = 2, 3, 4 and 6, respectively. Thus, sufficiently long polymers were obtained with more or less similar molar weight.

Solution processability

The undoped mTFF-C*n*SISC_2F_5 polymers are generally soluble in polar organic solvents, such as acetonitrile (ACN), tetrahydrofuran (THF), nitromethane (NM), propylene carbonate (PC), dimethylformamide (DMF) and dimethylsulfoxide (DMSO). Thus, the variation in tether length over the selected range does not significantly alter the solubility characteristics of the polymers.

Hygroscopicity

The undoped polymers were evaluated using a ''segmented thermogravimetry'' protocol with repeated measurements, as

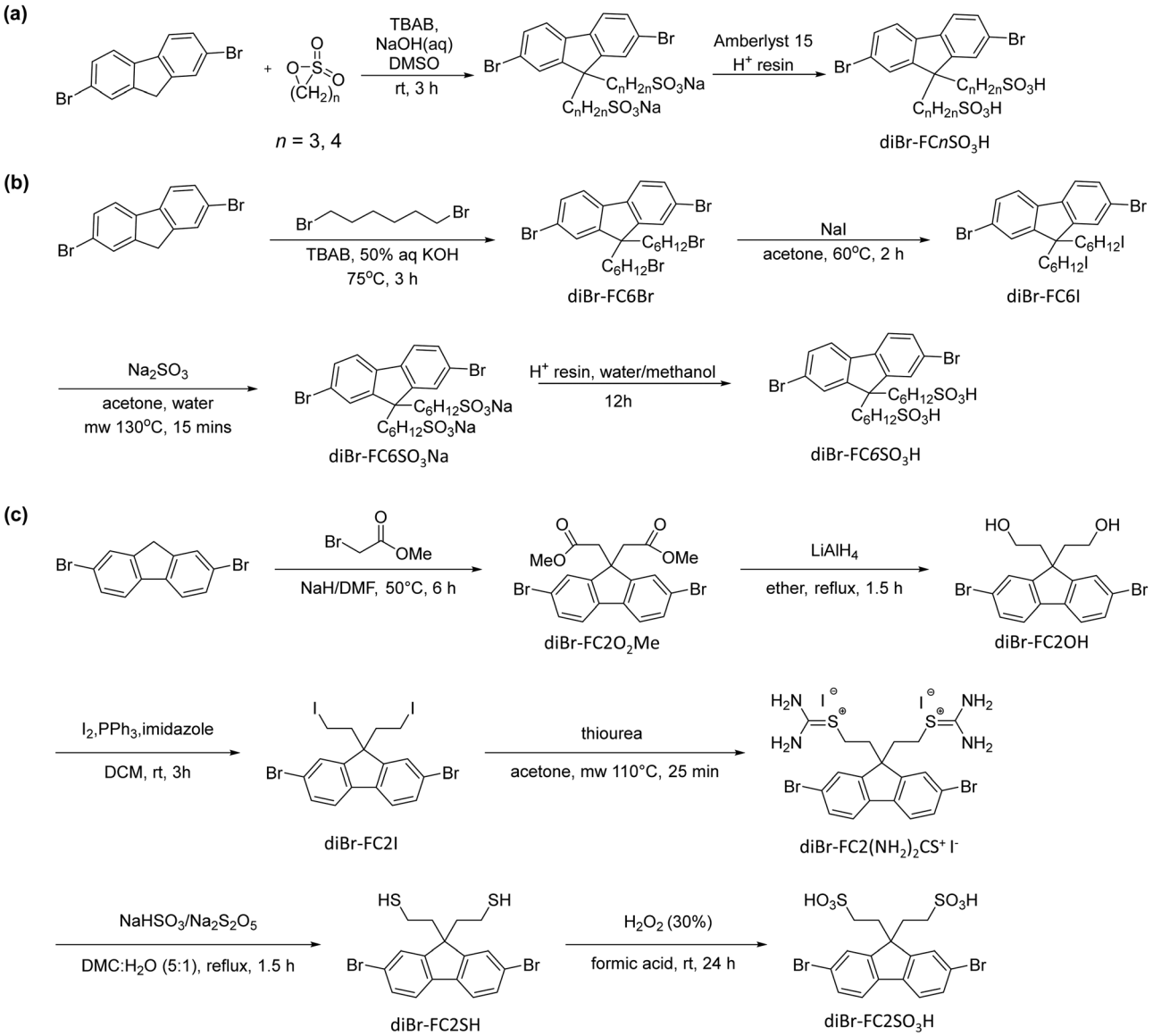

Scheme 1 (a) Synthesis path for **diBr-FC*n*SO$_3$H**. 1,3-Propanesultone is used for n = 3; 1,4-butanesultone is used for n = 4. (b) Synthesis path for **diBr-FC6SO$_3$H**. (c) Synthesis path for the **diBr-FC2SO$_3$H** monomer.

described in ref. 19. The thermograms are shown in Fig. 2. They exhibit three distinct weight loss steps, confirming the presence of three types of sorbed water as expected:[19] type-I water desorbing below 35 °C, type-II water between 35 °C and 130 °C, and type-III water (present only in the first scan) between 130 °C and 230 °C. These water species correspond to hydrogen-bonded water in the secondary hydration shell, anion-bound water in the primary hydration shell – located at the surface of the ion clusters – and caged water, respectively.[19] The hydration number for type-I water was found to be $n_w \approx 1.0$ H_2O per ion pair, independent of tether length (data taken from the second scan), but this is a significant underestimate.[19] In contrast, the hydration number for type-II water decreases systematically with tether length, that is, n_w decreases from 0.54 to 0.15 H_2O per ion pair as the tether length increases from n = 2 to 6. The hygroscopicity of a polyelectrolyte depends not only on the nature of the ion pair, but also on the morphology of the ion cluster formed by the ion pair.[19] The observed trend here suggests that the effective surface area per ion pair in the ion cluster decreases as its tether becomes longer. This indicates that the ions can assemble into larger aggregates with increasing tether length.

Hole doping

The hole-doped polymers were generated by quantitative oxidation with nitrosonium hexafluoroantimonate ($NOSbF_6$) or tris-(*p*-bromophenyl)aminium hexachloroantimonate ($TBPASbCl_6$; also known as "Magic Blue") in a nitrogen glovebox. We call this the "solution doping" method. Both NO^+ and $TBPA^{\bullet+}$ are strong one-electron oxidants (ε° (*vs.* SCE) in ACN: $NO^+/NO^\bullet$, 1.26 V; $TBPA^{\bullet+}$/TBPA, 1.06 V). All the hole-doped polymers, except **mTFF-C6SISC$_2$F$_5$**, are soluble in polar solvents,

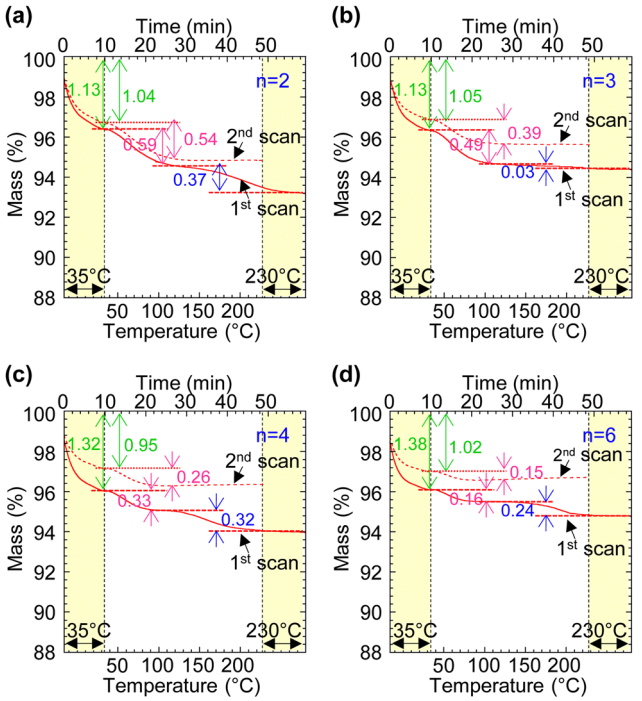

Fig. 2 Thermogravimetry analysis of mTFF-C*n*SISC$_2$F$_5$ powders. (a) n = 2, (b) 3, (c) 4, and (d) 6. After the first scan (solid line), the sample was cooled to room temperature, equilibrated under ambient conditions for 2 h, and reloaded into the thermoanalyzer for a second scan (dashed line). Conditions: ramp rate, 5 K min^{-1}; atmosphere, N_2. The weight loss steps correspond to water desorption: type-I water (below 35 °C, green annotation), type-II water (35–130 °C, magenta), and type-III water (130–230 °C, blue). The corresponding hydration number is annotated in the plot (n_w in H_2O per ion pair). Note that n_w for type-I H_2O content is significantly underestimated due to rapid desorption in N_2 during the thermoanalyzer dead time.

including ACN, NM and PC, which have sufficiently high oxidation potentials to be compatible with the doped polymers. However, hole-doped **mTFF-C6SISC$_2$F$_5$** undergoes gelation when oxidized by 0.7 equivalent or more of $NOSbF_6$, which cannot be overcome by dilution or heating. We speculate that this gelation arises from intrachain charge compensation, which binds the C_2F_5SIS anion to the doped hole, raising the overall hydrophobicity of the polymer. Thus, near-saturation hole-doped **mTFF-C6SISC$_2$F$_5$**, *i.e.* with a doping level (DL) near to the maximum value of 1 hole per repeat unit (h^+ per r.u.), cannot be obtained by solution doping. In contrast, near-saturation hole-doped mTFF-C*n*SISC$_2$F$_5$ can be readily obtained for n between 2 and 4 inclusive. Their SC forms were then generated through purification by repeated precipitation–redissolution cycles, during which the DL of the polymer drops marginally.

The near-saturation hole-doped state can also be generated by a different approach called the "film doping" method. This method involves contacting a cast film of the undoped polyelectrolyte with a dilute solution of the dopant, *e.g.*, 0.4 mM $TBPASbCl_6$ in 1 : 10 ACN : dimethyl carbonate (DMC), in a nitrogen glovebox. DMC is a nonsolvent for both undoped and hole-doped states of the polymer. Nevertheless, the presence of ACN in the solvent mixture is sufficient to swell the film, facilitating chemical injection of holes and in-diffusion of counteranions, *i.e.*, $SbCl_6^-$. The SC forms were then generated through purification by a spin-rinse cycle to remove the excess counteranions and spectator cations as $NaSbCl_6$, during which the DL of the polymer also drops marginally.

Electronic spectroscopy

We compared the UV-Vis-NIR spectra of the polymer films to evaluate their DL and whether the tether length influences disorder in the film (Fig. 3). Doping of TAF polymers leads to bleaching of the N1 and N2 absorption bands of the neutral polymer segments, and formation of the P1, P2 and P3 polaron absorption bands. The one-electron excitations that contribute to these transitions have been reported in ref. 17. The results here show that increasing tether length induces a small blueshift of the N1 absorption band (at *ca.* 3.3 eV), which is a HOMO → LUMO excitation of the neutral polymer (*i.e.*, undoped) segments, from the triphenylamine unit to the flanking fluorene units. The blueshift is *ca.* 100 meV from C2 to C6. In contrast, the blueshift is only 10–20 meV when dioctyl side chains on the fluorene unit are substituted by C3SISCF$_3$M side chains.[17] Thus, the larger blueshift here cannot be attributed solely to further changes in polarizability. Instead, it is attributed to assembly of the $C_2F_5SIS^-$ M^+ ion pairs into larger clusters with tether

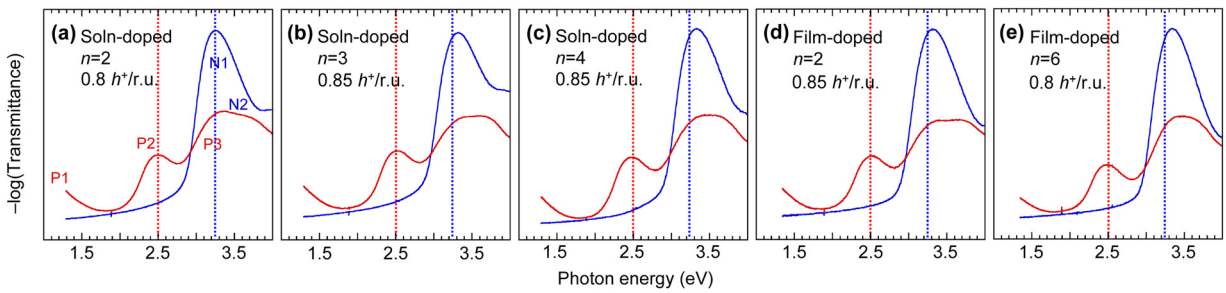

Fig. 3 Electronic spectroscopy of mTFF-C*n*SISC$_2$F$_5$ films in the neutral and nearly saturation hole-doped state. Solution-doped films: (a) n = 2, (b) 3, and (c) 4; and film-doped films: (d) n = 2 and (e) 6. Spectra: (blue) neutral, (red) hole-doped, with doping level in hole per repeat unit annotated. Vertical dotted lines as guide-to-the-eye: (blue) 3.25 eV and (red) 2.50 eV, aligned to peak centres in (a). 25–35-nm-thick films were prepared by spin-casting on O_2-plasma-cleaned quartz substrates in a nitrogen glovebox.

lengthening, which causes stronger twisting of the polymer backbone, *i.e.*, increasing its dihedral angles.

The P2 polaron absorption band (at *ca.* 2.5 eV) corresponds to a HOMO → LUMO excitation of the hole-doped segments, admixed with HOMO−*m* → SOMO* excitations.[17] This band redshifts *ca.* 30 meV from C4 to C6, which suggests that the conformational order of the hole-doped polymer backbone improves with tether length. The DL can be accurately evaluated from the intensities of the N1 and P2 bands relative to those of the undoped film and an authentic fully doped film (without the purification step) as ref. 17. Thus, the SC hole-doped films were found to exhibit a DL of 0.80–0.85 h^+ per r.u. The polaron spectra are practically identical for solution-doping and film-doping methods for the same polymer. Thus, the electronic state does not strongly depend on the method of doping.

Atomic force microscopy analysis reveals that both solution-doped and film-doped samples exhibit similar surface morphologies (Fig. S1, ESI†). The surfaces are smooth, with a root-mean-square roughness of *ca.* 10 Å. Thus, both solution-doping and film-doping methods can produce high-quality doped films.

Surface composition

We characterized the surface compositions of the films by X-ray photoemission spectroscopy (Fig. 4). This allows evaluation of the chemical species and DL present at the film surface. The atomic stoichiometries of the undoped films are in good agreement with theory (±10 atom%), except for carbon, which is high by *ca.* 20% (Table 1). The shapes of the C1s, S2p and F1s spectra do not change significantly with tether length. The enhanced detection of carbon indicates that the probed surface

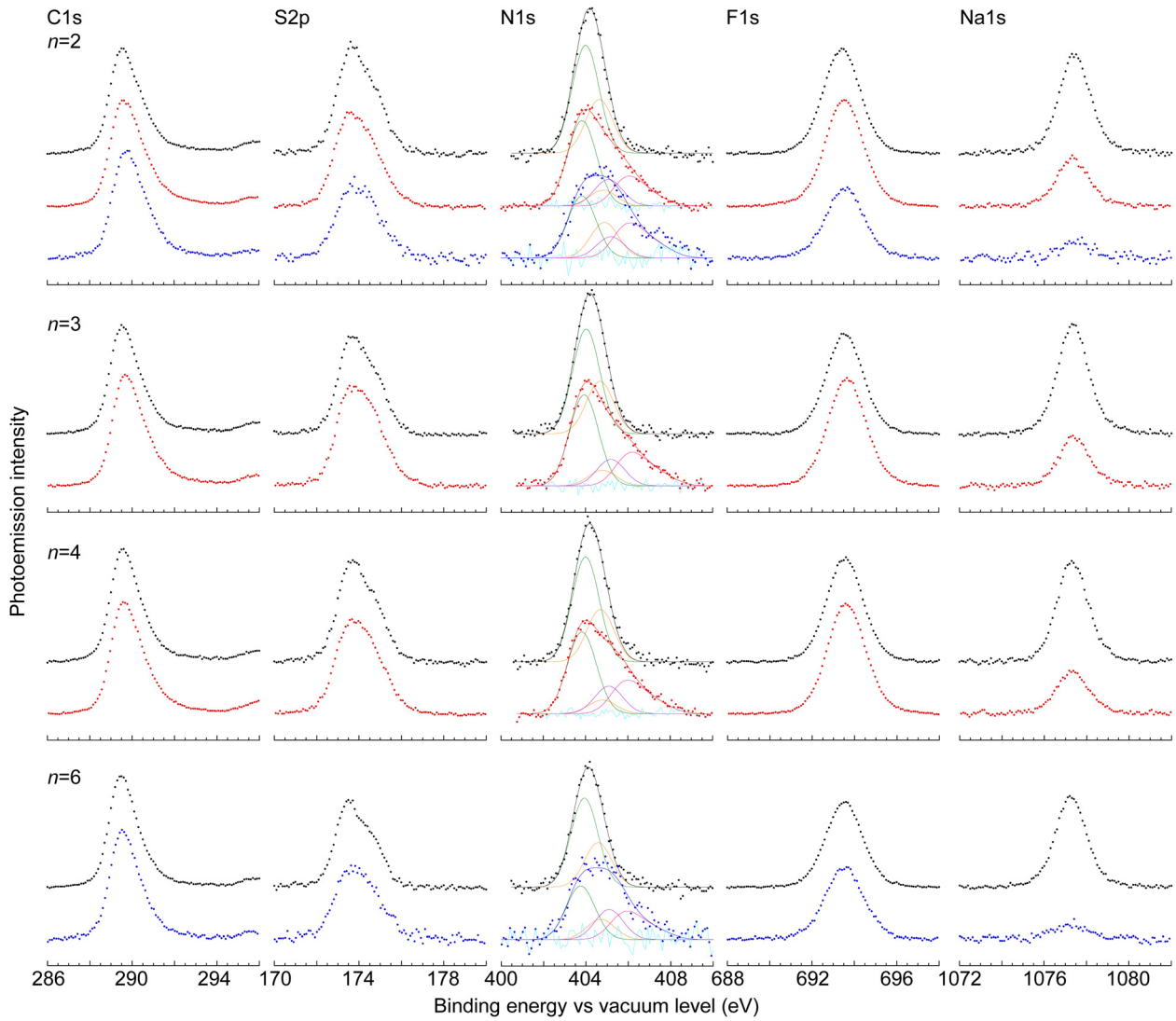

Fig. 4 Core-level X-ray photoemission spectra of undoped and self-compensated, saturation-hole-doped mTFF-C*n*SISC_2F_5 films. C1s, S2p, N1s, F1s and Na1s spectra plotted against binding energy measured from the vacuum level, for n = 2 (top panel), 3, 4, and 6 (bottom panel). Legend: circles, data – (black) undoped polymer, (red) solution-doped polymer, (blue) film-doped polymer. The N1s spectra were self-consistently fitted with components representing different species in the surface layer of the film: (green) C_2F_5SIS anion, (magenta) protonated C_2F_5SIS, (violet) amine, and (magenta) aminium moieties.

layer (*ca.* 25 Å deep) is selectively enriched with the polymer backbone relative to the C_2F_5SIS anion.

The N1s peak of the C_2F_5SIS anion emerges at *ca.* 404.15 eV in the undoped film, and that of the triphenylamine moiety at 404.6 eV. Doping broadens the N1s envelope: the C_2F_5SIS anion peak downshifts to 403.8 eV, the amine peak upshifts to 404.8 eV, and a new peak emerges at a higher binding energy of 405.85 eV, with strong tailing towards even higher binding energy. This last species is characteristic of the triphenylaminium moiety. Curve-fitting reveals an additional fourth component at 405.1 eV, which we assign to the protonated C_2F_5SIS species. Thus, we deconvolute the N1s spectrum into four components, corresponding to the C_2F_5SIS anion (denoted "N(−1)"), protonated C_2F_5SIS ("NH"), amine ("N(0)") and aminium ("N(+1)"). The area ratio of the curve-fitted aminium to the total amine and aminium, *i.e.*, [N(+1)]/([N(+1)] + [N(0)]), gives the DL at the film surface. Thus, the SC hole-doped films were found to exhibit a DL of 0.75–0.80 h^+ per r.u. at their surfaces, which is marginally lower than the DL in the bulk of the film.

XPS reveals a significant difference between the solution-doped and film-doped samples. While solution doping and self-compensation reduce the amount of Na^+ to half of its original value, as expected, film doping and self-compensation reduce the amount much more to 10–20% of its original value. Furthermore, excess amine and aminium species emerge (Table 1). These results indicate the displacement of Na^+ by $TBPA^{\bullet+}$ at the film surface. The surface binding of $TBPA^{\bullet+}$ to polyelectrolyte films has previously been established and utilized to introduce dopants for monolayer doping of organic semiconductor interfaces.[23] This $TBPA^{\bullet+}$ is expected to oxidize moisture over time, releasing H^+ to protonate the C_2F_5SIS anion. The products of this reaction are detected, TBPA and $SO_2NHSO_2C_2F_5$ as N(0) and NH, respectively. Thus, while both solution doping and film doping can yield high quality hole-doped films, the latter tends to bind excess oxidant to the film surface.

Table 1 Atomic stoichiometry ratio in the surface layer of the mTFF-C*n*SISC_2F_5 films ($3\lambda \approx 25$ Å). The ratio of SISC_2F_5 anion to triphenylamine is 2 : 1, as theoretically expected. N(+1) is triarylamininium, fitted with an asymmetric bandshape function with tailing towards higher binding energy, defined by a fundamental component at 405.85 eV and two higher components at 0.9 eV (45% of fundamental) and 1.8 eV (25% of fundamental). N(0) is triarylamine, at 404.8 eV. N(−1) is C_2F_5SIS anion, at 403.8 eV. NH is protonated C_2F_5SIS, at 405.1 eV. The doping level is 75–80%, slightly lower than that in the bulk. Film-doped films bind $TBPA^{\bullet+}$ to the surface, which contributes 'excess' intensity to N(+1) and N(0) components, the latter due to inadvertent reduction. Atomic stoichiometry ratios are normalized to S2p = 4.0. Theoretical ratios for the undoped polymers are C : S : F : Na : N = *m* : 4 : 13 : 2 : 3, where *m* = 40, 42, 44, and 48, for *n* = 2, 3, 4, and 6, respectively

						N1s: C_2F_5SIS-		N1s: amine	
n	C1s	S2p	F1s	Na1s	N1s	N(−1)[a]	NH[b]	N(0)[c]	N(+1)[d]
Undoped									
2	49	4.0	12	2.0	2.8	1.8	—	0.9	—
3	51	4.0	12	2.3	2.9	1.9	—	0.95	—
4	52	4.0	12	2.0	2.8	1.8	—	0.9	—
6	58	4.0	12	2.2	3.0	1.9	—	0.95	—
Solution-doped									
2	49	4.0	12	1.0	3.0	1.55	0.45	0.25	0.75
3	51	4.0	11	0.8	2.9	1.45	0.4	0.25	0.75
4	52	4.0	12	0.8	2.9	1.45	0.45	0.25	0.8
Film-doped									
2	52	4.0	10	0.25	3.9	1.45	0.5	0.8	1.15
6	57	4.0	11	0.4	3.4	1.3	0.7	0.45	0.95

Footnotes: relative binding energies. [a] N(−1) BE, *ca.* 403.8 eV. [b] NH BE, *ca.* 405.1 eV. [c] N(0) BE, *ca.* 404.8 eV. [d] N(+1) BE, *ca.* 405.85 eV.

Vacuum work function

We characterized the work function φ and valence band structure of the films using ultraviolet photoemission spectroscopy. The spectra of the undoped films show the HOMO band, which arises from the triphenylamine units, and the HOMO−1 band, which arises from the fluorene units (Fig. 5a).[14,17] The work function is given by $\varphi = E_{k,LECO} + h\nu - E_{k,FL}$, where $h\nu$ is the photon energy (He I, 21.22 eV), and $E_{k,FL}$ and $E_{k,LECO}$ are the kinetic energies of the photoelectrons emitted from the Fermi level (FL) established by a sputtered-clean Au reference and at the low-energy cutoff (LECO) of the film, respectively.

Hole doping bleaches out the HOMO band and deepens the Fermi level (Fig. 5b). Thus, the solution-doped SC films exhibit φ values of *ca.* 5.75 eV, which show a weak increasing trend from C2 to C4. These φ values are midway between those of mTFF:SbF_6, counterbalanced by the small SbF_6^- (3.35-Å radius), and mTFF:BArF, counterbalanced by the large tetrakis(3,5-bis(trifluoromethyl)phenyl)borate anion (8-Å radius) (Fig. 5d).[14] In general, φ increases weakly with DL in the heavily doped regime, but strongly with counteranion size due to loss of Madelung stabilization.[14] The tethered C_2F_5SIS anion here contacts the hole on the triphenylaminium unit over a distribution of distances between 4.5 and 6.5 Å (*vide infra*) due to its shape, orientation and tether, which gives apparent radii between 3.2 and 5.2 Å. This explains the enhanced φ values.

On the other hand, the film-doped SC films exhibit significantly lower φ values of *ca.* 5.55 eV. The shape and position of their valence band are practically identical to those of the solution-doped films, but their Fermi level is *ca.* 0.2 eV shallower (inset, Fig. 5b). This rules out any loss of doping or formation of unfavourable dipole at the surface, but indicates closer packing of counteranions to give stronger stabilisation of the holes (Fig. 5c). Thus, the counterions seem to relax more completely about the holes for film doping than solution doping. Yet, the lack of φ dependence on tether length suggests that the packing of these counterions does not change markedly with tether length within each doping method (Fig. 5d).

Molecular modeling: isolated repeat units

To investigate the charge-compensation structure of the counterions theoretically, we computed the PM3 molecular model of the hole-doped polymer repeat unit in the gas phase (Fig. 6; bond lengths and angles in Table 2). These calculations reveal that the tethered C*n*SISC_2F_5 anions position nearer to one edge of the polymer backbone due to their 9,9-fluorene attachment. This would enhance the visibility of the polymer backbone to XPS, as found experimentally. The calculations also reveal that

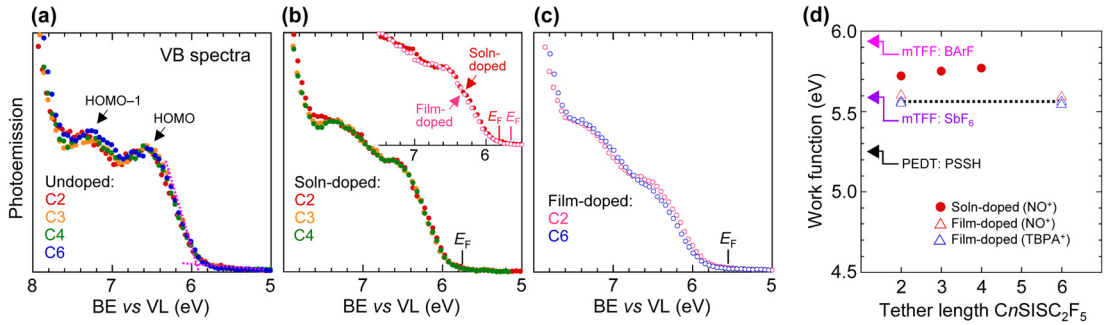

Fig. 5 Ultraviolet photoemission spectra of undoped and self-compensation, near-saturation hole-doped mTFF-CnSISC$_2$F$_5$ films. (a) Undoped, (b) solution-doped and (c) film-doped. The inset in (b) compares the solution-doped with a film-doped C2 sample fabricated in the same run. The film-doped sample shows the VB downshifts (*i.e.*, away from the vacuum level) by 0.05 eV but the Fermi level (E_F) upshifts by 0.2 eV. (d) Plot of work function against tether length. The doping level is 0.75–0.8 h^+ per r.u. for all films. Work functions of near-saturation hole-doped mTFF counterbalanced by BArF and SbF_6 are also shown for reference.

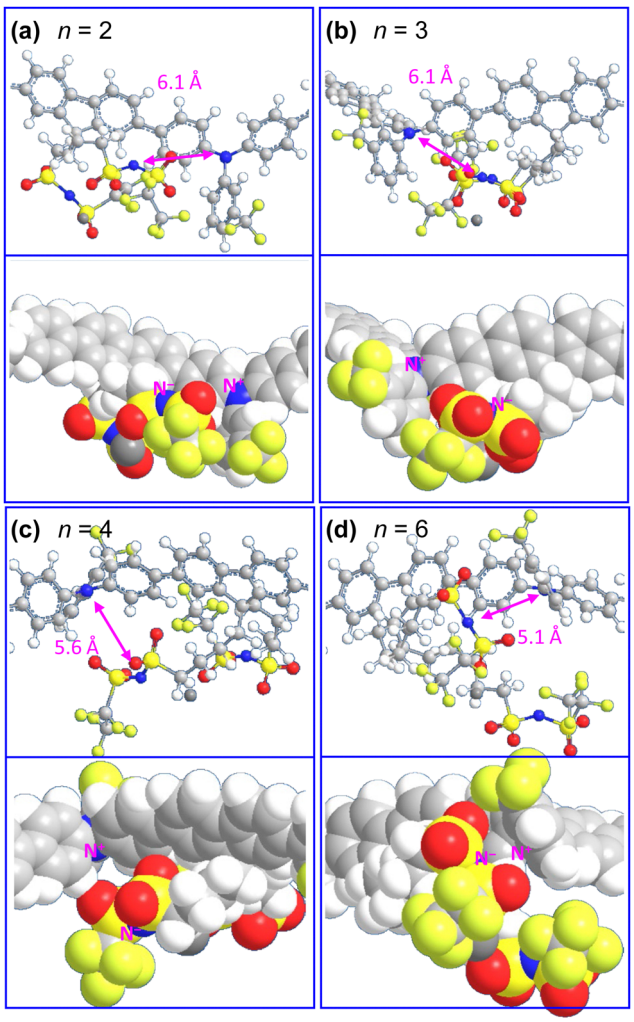

Fig. 6 Representative PM3 molecular models for the mTFF-CnSISC$_2$F$_5$ intra-chain self-compensated hole-doped state. (a) n = 2, (b) 3, (c) 4, and (d) 6. Atom legend: (grey) carbon, sodium; (white) hydrogen; (blue) nitrogen; (red) oxygen; (yellow) fluorine, sulfur. Ball-and-stick model and space-filling model.

the C2 and C3 tethers are not long enough for the C_2F_5SIS imide nitrogen to contact the triphenylaminium unit, but the C6 tether is long enough, *i.e.*, the N(+1)···N(−1) distance decreases to *ca.* 5 Å, depending on the conformation of the tether. Thus, intrachain charge compensation, where the counterion is tethered to the same polymer, may occur in the solid film for the C4 and C6 tethers, but not the shorter ones. Interchain compensation, where the counterion is tethered to an adjacent polymer, must thus occur for the shorter tethers.

Table 2 Comparison of PM3 and OPLS4 bond lengths and angles for the R–SIS–R_F side chain. R denotes alkyl, R_F denotes perfluoroalkyl

R-SIS-R_F	PM3 length (Å)	OPLS4 length (Å)
R: C–C	1.52	1.55
R: C–SO_2	1.82	1.88
RSO_2–N (imide)	1.68	1.54
(imide) N–SO_2R_F	1.64	1.56
R_F: SO_2–C	2.03	1.92
R_F: C–C	1.61	1.54

R-SIS-R_F	PM3 angle (°)	OPLS4 angle (°)
R: C–C–C	112	120
R: C–SO_2–N	101	103
SO_2–N (imide)–SO_2	143	120
R_F: N–SO_2–C	102	107

Molecular modeling: solid state

To investigate the crossover from interchain to intrachain compensation, we computed the polymer morphology in the amorphous solid state using the OPLS4 force field,[24] and extracted the pair correlation functions $g(r)$, as shown in Fig. 7a. The results reveal that the imide nitrogen and the Na^+ spectator cation are distributed over a range of distances from the hole (aminium nitrogen). The holes are indeed counterbalanced exclusively by interchain anions for the C2 and C3 tethers, but a mixture of intrachain and interchain anions for C4 and C6 tethers (Fig. 7b). As the tether length increases, it appears that interchain compensation dominates again, presumably due to entropy effects. The closest approach counteranion distance is *ca.* 4.5 Å for the C2 and C3 tethers, but *ca.* 4.9 Å for the C4 and C6 tethers due to stronger ion clustering with associated Na^+ distribution.

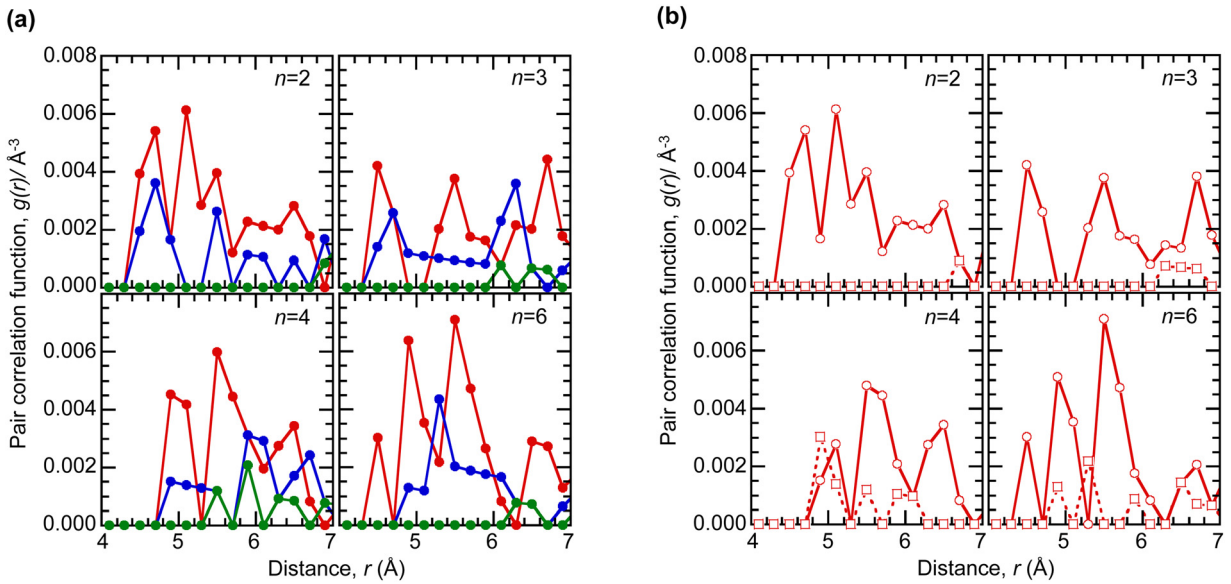

Fig. 7 OPLS4 molecular dynamics simulation of saturated-doped SC mTFF-C*n*SISC$_2$F$_5$. (a) Pair correlation functions $g(r)$ for triphenylaminium nitrogen: red, to C$_2$F$_5$SIS imide nitrogen; blue, to Na$^+$; and green, to next triphenylaminium nitrogen. (b) $g(r)$ for triphenylaminium nitrogen: open circles, to C$_2$F$_5$SIS imide nitrogen tethered to the adjacent chain (interchain compensation); open squares, tethered to the same chain (intrachain compensation).

As a consequence, the electrochemical potential of the holes due to the ion distribution[14,25] turns out to vary little with tether length. To estimate the local Madelung potential at the hole site, we computed.

$$E = \frac{e^2}{4\pi\varepsilon_o\varepsilon_r}\int_0^{R_s} 4\pi r(-g_{\text{h-an}}(r) + g_{\text{h-cat}}(r) + g_{\text{h-h}}(r))\mathrm{d}r$$

where h is the hole, an is the anion and cat is the cation, ε_r is the local dielectric constant (taken to be 3.0), and R_s is the continuum cut-off distance, taken to be 8.5 Å in these amorphous systems. The contributions of ions located further away than R_s can be neglected. Despite the relatively poor counting statistics, we can still estimate the local Madelung potentials to be −0.21, −0.12, −0.14 and −0.20 eV for n = 2, 3, 4 and 6, respectively. Thus, the hole energies are constant to within ±0.05 eV, possibly slightly more negative for the C2 and C6 tethers, which would correspondingly lower φ for these two tethers, in broad agreement with experiment. Thus, interchain self-compensation is confirmed for the shorter tethers.

Effective work function and PFOP diode characteristics

To check whether the high φ values of mTFF-C*n*SISC$_2$F$_5$ as the hole injection layer (HIL) persist in devices, we measured the built-in potential (V_{bi}) and current density–voltage (JV) characteristics of diodes fabricated with poly(9,9-bis(4-octylphenyl)fluorene-2,7-diyl) as the semiconductor (PFOP, I_E 5.8 eV; chemical structure in the inset of Fig. 9) and Al as the opposite electrode in the following structure: glass/ITO/30-nm HIL/90-nm PFOP/Al. This experiment provides a demanding test of the ability of the HIL to form ohmic hole contacts. We measured the dc-bias dependent Stark spectrum of the polymer,[26,27] as well as the subgap absorption spectrum from electroabsorption.[28] The modulated reflectance spectra $\Delta R/R$ varies linearly with the applied dc bias (V_{dc}), where ΔR is the modulated root-mean-square reflectance and R is the dc reflectance (Fig. 8). This shows that V_{bi} is well-behaved, which enables its accurate determination from the interpolated V_{dc} required to null the Stark absorption feature. A well-behaved V_{bi} in turn indicates well-behaved electrode φ values inside the devices.

Thus, the diodes with solution-doped mTFF-C*n*SISC$_2$F$_5$ films having a φ of *ca.* 5.75 eV were found to exhibit V_{bi} values of 2.40 ± 0.05 V. V_{bi} relates to the difference in effective φ between the anode and cathode contacts: $eV_{bi} = \varphi_{an} - \varphi_{cat}$.[29] Thus, the effective φ of the contact under study can be evaluated if the effective φ of the other contact is known.[29] Since the effective φ of the Al contact with PFOP (φ_{cat}) is 3.30 ± 0.05 eV,[29] the effective φ of the HIL inside the diode is evaluated to be 5.70 ± 0.07 eV, given by $\varphi_{an} = eV_{bi}$ + 3.30 eV, which agrees with the φ value measured by UPS. This finding affirms two conclusions: (1) the work function of the film does not change in the device and (2) the Fermi level of the HIL can closely approach the HOMO band edge of the PFOP test semiconductor. The latter conclusion corresponds to shallow Fermi level pinning, similar to the situation at the electron contact.[2] Shallow pinning provides better energy alignment for hole injection. Indeed, the strong modulated subgap absorption over the spectral range of 2.1–2.8 eV reveals the accumulation of a high density of holes in a δ-doped layer at the PFOP interface.[28] The subgap absorption is one order of magnitude stronger than for poly(3,4-ethylenedioxythiophene):poly(styrenesulfonic acid) (PEDT:PSSH) HIL films.[30] This demonstrates that a true ohmic hole contact is indeed formed. The diodes with film-doped mTFF-C*n*SISC$_2$F$_5$ films having a φ of *ca.* 5.55 eV were found to exhibit V_{bi} values of 2.15 V, which corresponds to an effective φ value for the HIL of 5.45 eV.

We demonstrate that the mTFF-C*n*SISC$_2$F$_5$ films with the high but not the low φ can efficiently inject holes into PFOP (Fig. 9). Diodes fabricated with solution-doped mTFF-C*n*SISC$_2$F$_5$

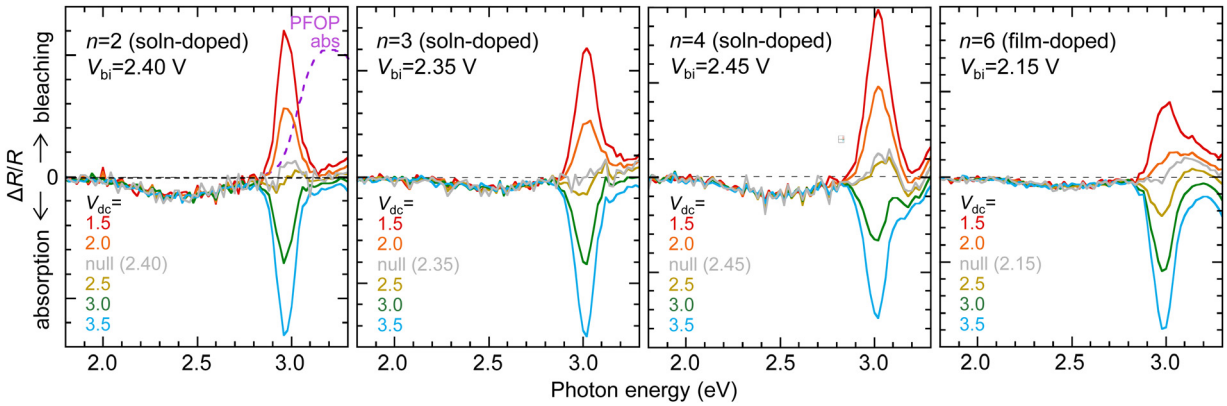

Fig. 8 Stark and subgap absorption by electroabsorption spectroscopy. Normalized reflectance spectra $\Delta R/R$ for ITO/hole-doped mTFF-C*n*SISC$_2$F$_5$/PFOP/Al. Upward features correspond to induced bleaching in-phase with the forward-bias half-cycle. The null spectrum is indicated by the grey line. Measurements were performed at 30 K, with a root-mean-square a.c. modulation of 0.5 V and a frequency of 535 Hz. The Stark peak occurs at 3.0 eV. The Fermi level of the Al/PFOP contact lies 3.3 eV below the effective vacuum level of PFOP.

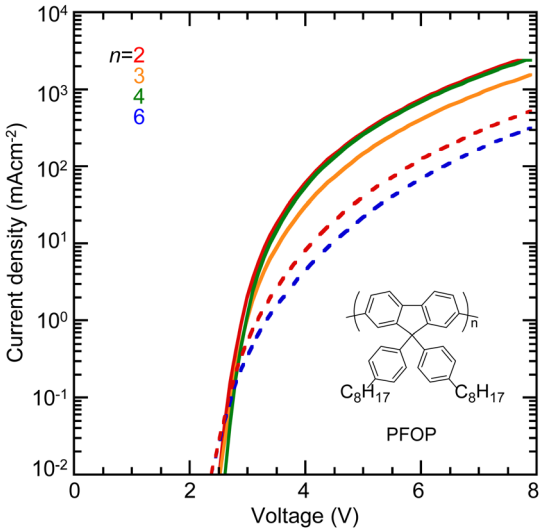

Fig. 9 *JV* curve of the hole-dominated PFOP diode with self-compensated hole-doped mTFF-C*n*SISC$_2$F$_5$ as the hole injection layer. Device structure: ITO/30-nm HIL/90-nm PFOP/Al. Data from the forward scan of a representative diode are shown. For solution-doped, n = 2 (red, solid); n = 3 (orange, solid); n = 4 (green, solid); for film-doped, n = 6 (blue, dash); n = 2 (red, dash). Inset: Chemical structure of PFOP.

HILs give the highest current density. Diodes with film-doped mTFF-C*n*SISC$_2$F$_5$ HILs give 80% lower current density. Earlier work with different TAF copolymers has shown that efficient hole injection is attained when φ exceeds about $I_E - 0.2$ eV, *i.e.*, the Fermi level of the doped organic electrode closely approaches or becomes deeper than the conventionally defined HOMO band edge of the semiconductor.[14,16]

Since the mTFF-*Cn*SISC$_2$F$_5$ HILs are bulk-doped, they form true ohmic contact that does not depend on confinement of opposite carriers.[31–33] In contrast, PEDT:PSSH modified with perfluorinated ionomers (PFI) can also give ultrahigh work functions due to surface segregation of an insulating PFI monolayer, but this imposes a tunnel barrier that impedes formation of a true ohmic contact under demanding conditions.[34]

Thermal stability

To evaluate the thermal stability of the SC hole-doped mTFF-C*n*SISC$_2$F$_5$ films, we measured the electronic spectra of the films as they are baked at increasing temperatures in a nitrogen glovebox. The results reveal that the C3-tether film can withstand short heating up to 120 °C but the others only up to 100 °C before thermal dedoping occurs (Fig. 10a). Nevertheless, hole-doped TAF polymers exhibit advantageously wide work function and conductivity plateaus. Their φ values lie within 80 meV of that of saturation doping for DL $\gtrsim$ 0.25 h$^+$ per r.u.[14] Their electrical conductivity values lie above 40% of the peak value for 0.25 $\lesssim$ DL $\lesssim$ 0.75 h$^+$ per r.u.[17] Thus, the minimum DL may be specified at 0.25 h$^+$ per r.u. for hole injection applications. For this threshold, mTFF-C*n*SISC$_2$F$_5$ films are able to tolerate short baking of up to 180 °C for the C6-tether film, and up to 210 °C for the C3-tether film, and temperatures between these two for the other films. Film doping gives similar stability results as solution doping, which suggests that thermal stability is determined by tether length rather than processing.

Ambient stability

The C2–C4-tether films also exhibit excellent ambient stability of their ultrahigh workfunction state despite the potential to oxidize moisture.[18] Their DL values are stable for up to 1 h under ambient conditions (22 °C, 65% relative humidity), which provides sufficient time for processing without protection by inert gas. But the DL values decline significantly after a few hours. The C3-tether film stabilizes at a DL of about 0.45 h$^+$ per r.u. after 1 month, which is remarkable for an ultrahigh-workfunction film.[18] Thus, the C3 tether confers best overall stability to the doped film. This conclusion also appears consistent with its marginally higher DL after self-compensation. The enhanced stability may be related to its ion

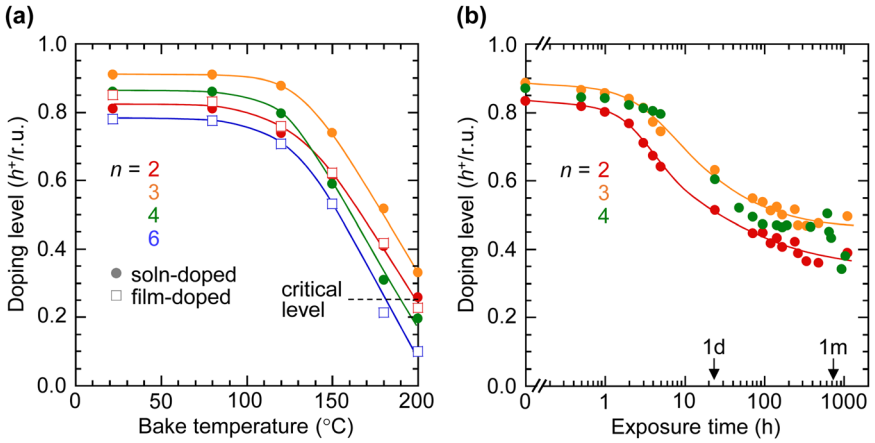

Fig. 10 Stability of self-compensated hole-doped mTFF-C*n*SISC$_2$F$_5$. (a) Thermal stability for 5-min bake at each temperature in the glovebox. (b) Ambient stability (22 °C, relative humidity 65%). Film thickness, 25–35 nm. Stability in the nitrogen glovebox is 100 times as long.

cluster morphology that may better exclude moisture while providing sufficient Coulomb stabilization for the holes.

Conclusion

In summary, we have designed, synthesized and characterized mTFF-C*n*SISC$_2$F$_5$ polymers with n = 2, 3, 4 and 6. We found that the material with the C6 tether becomes intractable in the fully hole-doped state, likely due to an enhanced hydrophobicity. The work function of the self-compensated hole-doped state can reach 5.75 eV, largely independent of tether length, which reflects a switchover from interchain to mixed interchain/intrachain self-compensation as the tether length increases, to maintain a similar local ion cluster environment in the vicinity of the holes. This enables unprecedentedly efficient hole injection from the hole-doped mTFF semiconductor core into PFOP. Yet, the C3 tether confers higher thermal and ambient stability than the other tethers, which we attribute to a more optimal ion cluster morphology.

Experimental

Materials

Poly(9,9′-bis(4-octylphenyl)fluorene-2,7-diyl) (PFOP) was obtained from Cambridge Display Technology Ltd/Sumitomo Chemical Co., Ltd.

Monomer synthesis

Synthesis of 1,4-phenylene-*N*-(*m*-trifluoro-methylphenyl)-amino-1,4-phenylene-4,4′-bis(pinacol)-diboronic ester (diEs-mTFF). To a 250-mL 2-neck round bottom flask (rbf) fitted with a reflux condenser, diphenylamine (10.15 g, 60 mmol), palladium(II) acetate (269.4 mg, 2 mol%), tri(*o*-tolyl)phosphine (730.5 mg, 4 mol%) and sodium *t*-butoxide (8.15 g, 85 mmol) were added. The rbf was pumped down to vacuum and backfilled with argon thrice. Anhydrous toluene (110 mL) was added to dissolve the solid. The reaction mixture was stirred under reflux at 110 °C for 12 h. Upon completion of reaction, the mixture was cooled to room temperature, filtered through a Celite layer and concentrated *via* rotary evaporation. The crude product was purified by column chromatography with hexane as the eluent to yield pure *N*,*N*-diphenyl-(*m*-trifluoromethyl)aniline (17.0 g, 91%). ^{1}H NMR (300 MHz, CDCl3), δ (ppm): 7.31–7.28 (m, 4H), 7.26–7.24 (m, 2H), 7.19–7,17 (m, 2H), 7.11–7.05 (m, 6H).

Into a 10-mL 1-neck rbf, *N*,*N*-diphenyl-(*m*-trifluoromethyl)-aniline (2.04 g, 6.52 mmol) and anhydrous dimethylformamide (DMF, 2.8 mL) were added. The reaction mixture was stirred under inert conditions for 15 min. *N*-Bromosuccinimide (2.44 g, 13.7 mmol) in anhydrous DMF (2.8 mL) solution was added dropwise into the rbf maintained at 5–7 °C. The reaction mixture was warmed to room temperature and stirred for 1 h, followed by precipitated in water. The crude product was extracted with hexane and dried over sodium sulphate. The extract was concentrated *via* rotary evaporation and purified by column chromatography with hexane as the eluent to yield pure *N*,*N*-di-*p*-bromophenyl-(*m*-trifluoromethyl)aniline (2.47 g, 81%). ^{1}H NMR (300 MHz, CDCl3), δ (ppm): 7.42–7.36 (m, 4H), 7.35–7.32 (d, 1H), 7.26–7.24 (m, 2H), 7.20–7.17 (d, 1H), 6.97–6.92 (m, 4H).

To a 250-mL 1-neck rbf, *N*,*N*-di-*p*-bromophenyl-(*m*-trifluoromethyl)aniline (5.0 g, 10.6 mmol) was added. The rbf was pumped down to vacuum and backfilled with argon thrice. Distilled tetrahydrofuran (THF, 70 mL) was added to dissolve the monomer. The reaction mixture was cooled to −78 °C before dropwise addition of 2.0 M *n*-butyl lithium in cyclohexane (12 mL, 24 mmol). The resulting reaction mixture was stirred at −78 °C for 2 h before the addition of 2-isopropoxy-4,4,5,5-tetramethyl-1,3,2-dioxaborolane (17 mL, 83.3 mmol). The reaction mixture was allowed to warm to room temperature and stirred for 24 h. The reaction was then quenched with water and concentrated *via* rotary evaporation. The crude product was extracted with dichloromethane (DCM) thrice and dried over sodium sulphate. Lastly, the extract was concentrated *via* rotary evaporation and purified by column chromatography with (19 : 1 ratio) hexane : ethyl acetate solvent mixture as the eluent to yield pure **diEs-mTFF** as a white solid (2.2 g, 37%). ^{1}H NMR (400 MHz, $CDCl_3$), δ (ppm): 7.72–7.69 (d, 4H), 7.36–7.31 (m, 2H), 7.26–7.22 (m, 2 H), 7.07–7.04 (d, 4H), 1.34 (s, 24H).

Synthesis of 9,9′-bis(methoxycarbonyl)methylene-2,7-dibromofluorene (diBr-FC2O$_2$Me). To a 250-mL 2-neck rbf, 2,7-dibromofluorene (5.18 g, 16 mmol) was added. The rbf was pumped down to vacuum and backfilled with argon thrice. DMF (120 mL) was added to dissolve the solid. The solution was cooled in an ice-water bath before sodium hydride (1.6 g, 40 mmol) was added portion wise. The reaction was warmed up to room temperature after no further H_2 gas evolved. Methyl bromoacetate (3.8 mL, 40 mmol) was added dropwise and the reaction was heated at 50 °C for 6 h. The reaction was quenched with water at 0 °C. The crude product was extracted with ethyl acetate thrice, washed with brine and dried over sodium sulphate. The extract was concentrated *via* rotary evaporation. Recrystallisation with methanol (MeOH) afforded **diBr-FC2O$_2$Me** as light orange crystals (5.88 g, 78.5%). ^{1}H NMR (400 MHz, DMSO-d$_6$), δ (ppm): 7.83 (d, 2H), 7.79 (d, 2H), 7.53 (dd, 2H), 3.27 (s, 6H), 3.20 (s, 4H).

Synthesis of 9,9′-bis(hydroxyethyl)-2,7-dibromofluorene (diBr-FC2OH). To a 250-mL 1-neck rbf, lithium aluminum hydride (0.84 g, 22 mmol) was added. The rbf was pumped down to vacuum and backfilled with argon thrice. Ether (150 mL) was added into the rbf. In a separate 500-mL 2-neck rbf, diBr-FC2CO$_2$Me (4.68 g, 10 mmol) was added and the rbf was pumped down to vacuum and backfilled with argon thrice. Ether (100 mL) was added to dissolve the solid. The lithium aluminum hydride suspension was added to the diBr-FC2CO$_2$Me solution and the reaction mixture was refluxed for 1.5 h. The reaction was quenched with water at 0 °C and ether was removed by rotary evaporation. The crude product was extracted with ethyl acetate thrice, washed with brine and dried over sodium sulphate. The extract was concentrated *via* rotary evaporation and purified by column chromatography with 1 : 1 hexane : ethyl acetate solvent mixture as the eluent to yield pure **diBr-FC2OH** as a white solid (3.86 g, 93.7%). ^{1}H NMR (400 MHz, DMSO-d$_6$), δ (ppm): 7.78 (m, 4H), 7.53 (dd, 2H), 4.18 (t, 2H), 2.63 (m, 4H), 2.24 (m, 4H). ^{13}C NMR (400 MHz, CDCl$_3$), δ (ppm): 150.8, 138.5, 131.2, 126.7, 122.1, 121.7, 58.8, 52.2, 42.7.

Synthesis of 9,9′-bis(iodoethyl)-2,7-dibromofluorene (diBr-FC2I). To a 250-mL 1-neck rbf, iodine (1.6 g, 6.3 mmol) and triphenylphosphine (1.65 g, 6.3 mmol) were added. The rbf was pumped down to vacuum and backfilled with argon thrice. DCM (40 mL) was added to dissolve the solid. To another 10-mL 1-neck rbf, imidazole (0.49 g, 7.2 mmol) was added and the rbf was pumped down to vacuum and backfilled with argon thrice. DCM (6 mL) was added to dissolve the solid. To the third 150-mL 1-neck rbf, diBr-FC2OH (1.24 g, 3.0 mmol) was added and the rbf was pumped down to vacuum and backfilled with argon thrice. DCM (120 mL) was added to dissolve the monomer. The iodine/triphenylphosphine solution was stirred for 10 min before the imidazole solution was added to it. The solution of **diBr-FC2OH** was added and the reaction mixture was stirred for 3 h at room temperature. Upon completion of reaction, hexane was added and the solids were removed by filtration. The solution was concentrated *via* rotary evaporation and purified by column chromatography with 20 : 1 hexane : ethyl acetate solvent mixture as the eluent to yield pure diBr-C$_2$I as a white solid (1.39 g, 84.3%). ^{1}H NMR (400 MHz, DMSO-d$_6$), δ (ppm): 7.95 (d, 2H), 7.84 (d, 2H), 7.61 (dd, 2H), 2.72 (m, 4H), 2.28 (m, 4H). ^{13}C NMR (400 MHz, CDCl$_3$), δ (ppm): 148.1, 139.3, 131.8, 126.3, 122.5, 121.9, 59.4, 44.4, −2.66. HRMS (APCI) *m*/*z* 629.7548 (calcd for M$^+$ 629.7552).

Synthesis of 9,9′-bis(isothiouranium)ethyl-2,7-dibromofluorene iodide (diBr-FC2(NH$_2$)$_2$CSI). To a 20-mL microwave vial, **diBr-FC2I** (237 mg, 0.4 mmol) and thiourea (571 mg, 7.5 mmol) were added. The vial was crimp-sealed, pumped down to vacuum and backfilled with Ar thrice. Acetone (18 mL) was added. The vial was heated to 45 °C at which all solids dissolved. The vial was heated in a microwave at 110 °C for 25 min. The solution was concentrated by rotary evaporation and precipitated in DCM. The precipitate was re-dissolved in acetone and precipitated in DCM to yield the diBr-FC2(NH$_2$)$_2$CSI/thiourea mixture which was used for the next step without any further purification (72.0%). ^{1}H NMR (400 MHz, DMSO-d$_6$), δ (ppm): 8.78 (s, 8H), 7.89 (m, 4H), 7.64 (dd, 2H), 2.44 (m, 4H), 2.37 (m, 4H). HRMS (APCI) *m*/*z* 526.9565 (calcd for M$^+$ 526.9569).

Synthesis of 9,9′-bis(thioethyl)-2,7-dibromofluorene (diBr-C$_2$SH). To a 250-mL 2-neck rbf, the diBr-FC2(NH$_2$)$_2$CSI/thiourea mixture (450 mg, 0.23 mmol) and sodium bisulfite (1.18 g, 11 mmol) were added. The rbf was pumped down to vacuum and backfilled with argon thrice. DCM (110 mL) was added to dissolve the solid. Water (22 mL) was added and the solution mixture was refluxed for 1.5 h. Upon completion of reaction, the solution was diluted with DCM, washed with water twice, followed by brine, and dried over sodium sulphate. The solution was concentrated *via* rotary evaporation and purified by column chromatography with 3 : 1 hexane : ethyl acetate solvent mixture as the eluent to yield pure diBr-FC2SH as a white solid (82.8 mg, 80.1%). ^{1}H NMR (400 MHz, DMSO-d$_6$), δ (ppm): 7.83 (m, 4H), 7.58 (dd, 2H), 2.33 (m, 4H), 2.27 (t, 2H), 1.59 (m, 4H). ^{13}C NMR (400 MHz, CDCl$_3$), δ (ppm): 150.2, 138.6, 130.7, 126.4, 122.3, 121.3, 55.9, 42.6, 18.5. HRMS (APCI) *m*/*z* 440.8926 (calcd for M$^-$ 440.8987).

Synthesis of 9,9′-bis(ethylsulfonic acid)-2,7-dibromofluorene (diBr-FC2SO$_3$H). To a 50-mL 1-neck rbf, hydrogen peroxide (30%, 3 mL) was added. Formic acid (7 mL) was added at 0 °C and the mixture was stirred for 1 h. To another 10-mL 1-neck rbf, diBr-FC2SH (75 mg, 0.17 mmol) was added. The rbf was pumped down to vacuum and backfilled with argon thrice. Formic acid (5 mL) was added into the rbf to dissolve the monomer. The monomer solution was added dropwise into the mixture of hydrogen peroxide and formic acid. The solution mixture was stirred for 24 h and the solvents were removed *via* rotary evaporation to yield pure **diBr-FC2SO$_3$H** as an orange solid (36.2 mg, 56%). ^{1}H NMR (400 MHz, DMSO-d$_6$), δ (ppm): 7.83 (d, 2H), 7.65 (m, 2H), 7.57 (dd, 2H), 2.32 (m, 4H), 1.53 (m, 4H). HRMS (APCI) *m*/*z* 536.8686 (calcd for M$^-$ 536.8682).

Synthesis of 9,9′-bis(3′-pentafluoroethylsulfonylimidoethyl)-2,7-dibromofluorene triethylammonium salt (diBr-FC2SIS-C2F5-TEAH). To a 150-mL 2-neck rbf fitted with a stopcock valve adaptor, diBr-FC2SO$_3$H (1.00 g, 1.9 mmol) was added. The rbf was pumped down to vacuum and backfilled with argon thrice. Distilled THF (34 mL) was added to dissolve the monomer.

Catalytic anhydrous DMF (0.07 mL) was added, followed by dropwise addition of oxalyl chloride (3.2 mL, 38.0 mmol) and anhydrous chloroform (43 mL). The reaction was stirred at room temperature for 6 h. Upon completion of reaction, the 9,9′-bis(3′-chlorosulfonylethyl)-2,7-dibromofluorene (**diBr-FC2SO$_2$Cl**) intermediate was dried *in situ* under vacuum to remove all the solvents and excess oxalyl chloride, and re-dissolved in anhydrous chloroform (12.2 mL). In a separate rbf, pentafluoroethanesulfonamide (PFES, 7.4 g, 38.0 mmol) was mixed with anhydrous triethylamine (TEA, 5.2 mL, 38.0 mmol) in anhydrous chloroform (13 mL). This solution was then added to the solution of 9,9′-bis(3′-chlorosulfonylethyl)-2,7-dibromofluorene and left to stir at room temperature for 1 h. Upon completion of reaction, the reaction mixture was concentrated by rotary evaporation before precipitation in diethyl ether. The precipitate was re-dissolved in chloroform and precipitated in diethyl ether twice. The crude product was re-dissolved in chloroform and purified by extraction with water thrice. The organic phase was concentrated and then precipitated in diethyl ether, yielding pure 9,9′-bis(3′-pentafluoroethylsulfonylimidoethyl)-2,7-dibromofluorene triethylammonium salt (**diBr-FC2SISC2F5-TEAH**) as an off-white solid. ^{1}H NMR (400 MHz, DMSO-d$_6$), δ (ppm): 7.85 (d, 2H), 7.77 (d, 2H), 7.60 (dd, 2H), 3.09 (q, 12H), 2.47 (m, 4H), 2.03 (m, 4H), 1.17 (t,18H). ^{19}F NMR (400 MHz, DMSO-d$_6$), δ (ppm): −78.6 (s, 3F), −116.8 (s, 2F).

Synthesis of 9,9′-bis(3′-pentafluoroethylsulfonylimidopropyl)-2,7-dibromofluorene triethylammonium salt (diBr-FC3SISC$_2$F$_5$-TEAH). This was synthesized following the procedure by Tang *et al.* with some modifications in the purification steps.[1] To a 250-mL 2-neck rbf, 2,7-dibromofluorene (4.41 g, 13.6 mmol) and tetra-*n*-butylammonium bromide (89.2 mg, 2 mol%) were added. The rbf was pumped down to vacuum and backfilled with argon thrice. Dimethyl sulfoxide (DMSO, 80 mL) and 50 wt% sodium hydroxide solution (8.8 mL) were added. 1,3-Propanesultone (4.10 mg, 33.6 mmol) was dissolved in DMSO (22 mL) and added dropwise into the reaction mixture. The reaction mixture was stirred at room temperature for 3 h. Upon completion of reaction, the crude product was obtained by precipitation in acetone and washed with cold ethanol and cold acetone. The precipitate was recrystallized in water to give a crude solid. The recrystallized product was then re-dissolved in water and precipitated in acetone twice to give pure 9,9′-bis(3′-sulfonatopropyl)-2,7-dibromofluorene sodium salt (**diBr-FC3SO$_3$Na**) as a white solid (yield: 66%). ^{1}H NMR (400 MHz, D$_2$O), δ (ppm): 7.75–7.71 (m, 4H), 7.61–7.58 (dd, 2H), 2.63–2.58 (t, 4H), 2.23–2.17 (t, 4H), 1.05–1.02 (m, 4H). In a 100-mL Nalgene bottle, 3.5 g (5.7 mmol) of **diBr-FC3SO$_3$Na** was dissolved in MeOH. The Amberlyst 15 hydrogen form H$^+$ resin at 20 molar equivalents (24.3 g, 114.3 mmol) was washed to pH 7 with deionized water and pre-conditioned with MeOH overnight before adding to the solution. The solution was left on a mechanical roller for 6 h at room temperature. The solution was then filtered through a 0.45-μm nylon syringe filter into a 50-mL rbf. The solution was dried *via* rotary evaporation, yielding the 9,9′-bis(3′- sulfonatopropyl)-2,7-dibromofluorene acid form (**diBr-FC3SO$_3$H**) as a white solid. Upon drying, **diBr-FC3SO$_3$H** (2.47 g, 4.2 mmol) was added into a 150-mL 2-neck rbf fitted with a stopcock valve adaptor. The rbf was pumped down to vacuum and backfilled with argon thrice. Distilled THF (80 mL) was added to dissolve the monomer. Catalytic anhydrous DMF (0.25 mL) was further added, followed by dropwise addition of oxalyl chloride (7.1 mL, 84.0 mmol). The reaction was stirred at room temperature for 6 h. Upon completion of reaction, the 9,9′-bis(3′-chlorosulfonylpropyl)-2,7-dibromofluorene (**diBr-FC3SO$_2$Cl**) intermediate was dried *in situ* under vacuum to remove solvents and oxalyl chloride, and re-dissolved in anhydrous chloroform (40 mL). In a separate rbf, pentafluoroethanesulfonamide (PFES, 16.7 g, 84.0 mmol) was mixed with anhydrous triethylamine (TEA, 11.7 mL, 84.0 mmol) in anhydrous chloroform (30 mL). This solution was then added to **diBr-FC3SO$_2$Cl** solution and left to stir at room temperature for 1 h. Upon completion of reaction, the mixture was concentrated by rotary evaporation and precipitated in diethyl ether. The precipitate was re-dissolved in chloroform and precipitated in diethyl ether twice. The crude product was dissolved in chloroform extracted against deionized water thrice. The extract was precipitated in diethyl ether, filtered and washed with water and diethyl ether yielding pure 9,9′-bis(3′-pentafluoroethylsulfonylimidopropyl)-2,7-dibromofluorene triethylammonium salt (**diBr-FC3SISC$_2$F$_5$-TEAH**) as a white solid (4.5 g, yield = 95%). ^{1}H NMR (400 MHz, DMSO-d$_6$), δ (ppm): 7.82–7.78 (d, 2H), 7.70 (s, 2H), 7.57–7.54 (d, 2H), 3.12–3.07 (q, 12H), 2.74–2.71 (t, 4H), 2.12–2.08 (t, 4H), 1.20–1.16 (t,18H), 0.86–0.81 (m, 4H). ^{19}F NMR (400 MHz, DMSO-d$_6$), δ (ppm): −78.8 (s, 3F), −117.1 (s, 2F).

Synthesis of 9,9′-bis(3′-pentafluoroethylsulfonylimidobutyl)-2,7-dibromofluorene triethylammonium salt (diBr-FC4SISC$_2$F$_5$-TEAH). To a 250-mL 2-neck rbf, 2,7-dibromofluorene (4.41 g, 13.6 mmol) and tetra-*n*-butylammonium bromide (89.2 mg, 2 mol%) were added. The rbf was pumped down to vacuum and backfilled with argon thrice. DMSO (80 mL) and 50 wt% sodium hydroxide solution (8.8 mL) were added. 1,4-Butanesultone (3.4 mL, 33.6 mmol) was dissolved in DMSO (22 mL) and added dropwise into the reaction mixture. The reaction mixture was stirred at room temperature for 3 h. Upon completion of reaction, the solution was precipitated in acetone and washed with cold ethanol, followed by cold acetone to yield the crude product. The crude product was recrystallized in water. The recrystallized product was re-dissolved in MeOH and precipitated twice in acetone to yield pure 9,9′-bis(3′-sulfonatobutyl)-2,7-dibromofluorene sodium salt (**diBr-FC4SO$_3$Na**) as an off-white solid (yield: 66%). ^{1}H NMR (400 MHz, D$_2$O), δ (ppm): 7.80–7.74 (m, 4H), 7.65–7.59 (dd, 2H), 2.70–2.60 (t, 4H), 2.20–2.10 (t, 4H), 1.60–1.50 (m, 4H), 0.80–0.60 (m, 4H).

In a 100-mL Nalgene bottle, 3.5 g (5.5 mmol) of **diBr-FC4SO$_3$Na** was dissolved in MeOH. The Amberlyst 15 hydrogen form H$^+$ resin at 20 molar equivalents (23.3 g, 109.3 mmol) was washed to pH 7 with deionized water and pre-conditioned with MeOH overnight before adding to the solution. The solution was left on a mechanical roller for 6 h at room temperature. The solution was then filtered through a 0.45-μm nylon syringe filter into a rbf. The filtered solution was dried *via* rotary evaporation, yielding the 9,9′-bis(3′-sulfonatobutyl)-2,7-dibromofluorene acid form (**diBr-FC4SO$_3$H**) as an off-white solid. Upon drying, **diBr-FC4SO$_3$H** (2.50 g, 4.2 mmol) was added into a 150-mL 2-neck rbf fitted with a stopcock valve adaptor. The rbf was pumped down to vacuum and backfilled with argon thrice.

Distilled THF (80 mL) was added to dissolve the monomer. Catalytic anhydrous DMF (0.25 mL) was added, followed by dropwise addition of oxalyl chloride (7.1 mL, 84.0 mmol). The reaction was stirred at room temperature for 6 h. Upon completion of reaction, the 9,9′-bis(3′-chlorosulfonylbutyl)-2,7-dibromofluorene (**diBr-FC4SO$_2$Cl**) intermediate was dried *in situ* under vacuum to remove all solvents and oxalyl chloride, and re-dissolved in anhydrous chloroform (40 mL). In a separate rbf, pentafluoroethanesulfonamide (PFES, 16.7 g, 84.0 mmol) was mixed with anhydrous triethylamine (TEA, 11.7 mL, 84.0 mmol) in anhydrous chloroform (30 mL). This solution was added to **diBr-FC4SO$_2$Cl** solution and left to stir at room temperature for 1 h. Upon completion of reaction, the mixture was concentrated by rotary evaporation and precipitated in diethyl ether. The solid was re-dissolved in chloroform and precipitated in diethyl ether twice. The crude product was re-dissolved in chloroform extracted against deionized water. The organic phase was concentrated and then precipitated in diethyl ether, yielding pure 9,9′-bis(3′-pentafluoroethylsulfonylimidobutyl)-2,7-dibromofluorene triethylammonium salt (**diBr-FC4SISC$_2$F$_5$-TEAH**) as a brown oil (yield = 82%). ^{1}H NMR (400 MHz, DMSO-d$_6$), δ (ppm): 7.79–7.77 (d, 2H), 7.74–7.72 (d, 2H), 7.52–7.50 (d, 2H), 3.00–2.90 (q, 12H), 2.71–2.67 (t, 4H), 2.05–2.01 (t, 4H), 1.46–1.40 (m, 4H), 1.20–1.10 (t, 18H), 0.54–0.49 (m, 4H). ^{19}F NMR (400 MHz, DMSO-d$_6$), δ (ppm): −78.6 (s, 3F), −116.8 (s, 2F).

Synthesis of 9,9′-bis(3′-sulfonatohexyl)-2,7-dibromofluorene sodium salt (diBr-FC6SO$_3$Na). To a 150-mL 2-neck rbf, 2,7-dibromofluorene (2.00 g, 6.17 mmol) and tetra-*n*-butylammonium bromide (397 mg, 1.23 mmol) were added. The rbf was pumped down to vacuum and backfilled with argon thrice. 50 wt% potassium hydroxide solution (50 mL) was added, followed by 1,6-dibromohexane (9.49 mL, 61.7 mmol). The reaction mixture was heated to 75 °C and stirred for 3 h. Upon completion of reaction, the crude product was extracted with DCM followed by washing with 5% HCl and dried over sodium sulphate. The organic phase was concentrated *via* rotary evaporation and purified by column chromatography with hexane as the eluent to yield pure **diBr-FC6Br** as a solid. Upon drying, **diBr-FC6Br** (2.00 g, 3.1 mmol), potassium iodide (1.13 g, 6.8 mmol) and acetone (40 mL) were added into a 100-mL 1-neck rbf. The reaction mixture was stirred under reflux at 60 °C for 2 h. Upon completion of reaction, the crude product was extracted with DCM, followed by brine, and dried over sodium sulphate. The solution was dried *via* rotary evaporation to yield **diBr-FC6I** as a solid. To a 20-mL microwave vial, **diBr-FC6I** (1 g, 1.3 mmol), acetone (10.4 mL), and sodium sulfite (0.36 g, 2.9 mmol) dissolved in deionized water (3.9 mL) were added. The vial was crimp-sealed before heating in a microwave at 130 °C for 3 h. Upon cooling to room temperature, the crude product was dried *via* rotary evaporation and purified by washing with DCM and acetone. The purified solid was dissolved in MeOH and filtered to obtain a clear solution. The filtrate was collected and concentrated *via* rotary evaporation to yield 9,9′-bis(3′-sulfonatohexyl)-2,7-dibromofluorene sodium salt (**diBr-FC6SO$_3$Na**) as a white solid. ^{1}H NMR (400 MHz, D$_2$O-d$_6$), δ (ppm): 7.50–7.25 (m, 6H), 2.65–2.55 (m, 4H), 1.90–1.75 (m, 4H), 1.45–1.35 (m, 4H), 1.00–0.7 (m, 8H), 0.50–0.30 (m, 4H).

Synthesis of 9,9′-bis(3′-trifluoromethylsulfonylimidohexyl)-2,7-dibromofluorene triethylammonium salt (diBr-FC6SISC$_2$F$_5$-TEAH). In a 25-mL Nalgene bottle, **diBr-C$_6$SO$_3$Na** (722 mg, 1.04 mmol) was dissolved in 10 : 1 MeOH : H$_2$O (10 mL). The Amberlyst 15 hydrogen form H$^+$ resin at 20 molar equivalents (2.22 g, 10.4 mmol) was washed to pH 7 with deionized water and pre-conditioned with MeOH overnight before adding to the solution. The solution was left on a mechanical roller for 6 h at room temperature. The solution was then filtered through a 0.45-μm nylon syringe filter into a rbf and dried *via* rotary evaporation to yield the crude product as an orange solid. The crude solid was washed with hexane to yield the 9,9′-bis(3′-sulfonatohexyl)-2,7-dibromofluorene acid form (**diBr-FC6SO3H**) as an off-white solid. Into a 50-mL 2-neck rbf fitted with a stopcock valve adaptor, **diBr-FC6SO$_3$H** (200 mg, 0.3065 mmol) was loaded. The rbf was pumped down to vacuum and backfilled with argon thrice. Distilled tetrahydrofuran (3.4 mL) and anhydrous chloroform (3.4 mL) were added to dissolve the monomer. Catalytic anhydrous DMF (0.01 mL) was further added, followed by dropwise addition of oxalyl chloride (0.52 mL, 6.13 mmol). The reaction was stirred at room temperature for 6 h. Upon completion of reaction, the 9,9′-bis(3′-chlorosulfonylhexyl)-2,7-dibromofluorene (**diBr-FC6SO$_2$Cl**) intermediate was dried *in situ* under vacuum to remove all solvents and oxalyl chloride, and re-dissolved in anhydrous chloroform (3 mL). In a separate rbf, pentafluoroethanesulfonamide (PFES, 1.220 g, 6.13 mmol) was mixed with anhydrous triethylamine (TEA, 0.82 mL, 6.13 mmol) in anhydrous chloroform (3 mL). This solution was added to the **diBr-FC6SO$_2$Cl** solution and left to stir at room temperature for 3 h. Upon completion of reaction, the mixture was concentrated by rotary evaporation and precipitated in diethyl ether. The precipitate was re-dissolved in chloroform and precipitated twice in diethyl ether. The crude product was re-dissolved in chloroform and extracted against water and brine thrice. The extract was dried over sodium sulfate and precipitated in diethyl ether, yielding impure **diBr-FC6SISC$_2$F$_5$-TEAH** as a brown oil.

Synthesis of 9,9′-bis(3′-trifluoromethylsulfonylimidohexyl)-2,7-dibromofluorene triethylammonium salt (diBr-FC6SISC$_2$F$_5$-Na). In a 25-mL Nalgene bottle, 300 mg (1.04 mmol) of **diBr-FC6SISC$_2$F$_5$-TEAH** was dissolved in ACN (10 mL). The solution was filtered through a 0.45-μm nylon syringe filter to give a clear solution. 20 equivalents of Amberlyst 15 hydrogen form H$^+$ resins were ion-exchanged with 5 equivalents of sodium hydroxide (5 M, in water) overnight to yield Amberlyst 15 sodium form Na$^+$ resins (2.22 g, 10.4 mmol). The Na$^+$ resin was washed to pH 7 with deionized water and pre-conditioned with ACN overnight, and added to the **diBr-FC6SISC$_2$F$_5$-TEAH** solution. The solution was left on a mechanical roller for 48 h at room temperature. The solution was then filtered through a 0.45-μm nylon syringe filter into a rbf. The solution was dried *via* rotary evaporation, yielding crude **diBr-FC6SISC$_2$F$_5$-Na** as a sticky oil. The crude oil was dried under vacuum overnight to yield the crude **diBr-FC6SISC$_2$F$_5$-Na** solid. The crude solid was dissolved in ACN and filtered through a 0.45-μm nylon syringe filter. The solution was dried *via* rotary

evaporation, yielding pure 9,9′-bis(3′-pentafluoroethylsulfonylimidohexyl)-2,7-dibromofluorene sodium salt (**diBr-FC6SISC$_2$F$_5$-Na**) as an off-white solid. ^{1}H NMR (400 MHz, DMSO-d$_6$), δ (ppm): 7.80–7.75 (d, 2H), 7.72–7.69 (d, 2H), 7.56–7.48 (d, 2H), 2.85–2.76 (t, 4H), 2.01–1.74 (t, 4H), 1.52–1.37 (t, 4H), 1.17–0.89 (m, 8H), 1.20–1.10 (m, 18H), 0.50–0.32 (m, 4H).

Synthesis of poly(9,9′-bis(2-pentaethylsulfonylimidosulfonylethyl)fluorene-2,7-diyl-1,4-phenylene-*N*-(*m*-trifluoromethylphenyl)-imino-1,4-phenylene) sodium salt (mTFF-C2SISC$_2$F$_5$). Into a 20-mL microwave vial, equimolar portions of **diBr-FC2SISC$_2$F$_5$-TEAH** (500.00 mg, 0.45 mmol), **diEs-mTFF** (255.82 mg, 0.45 mmol) and catalytic Pd(dppf)Cl$_2$ (3 mol%) were added. The vial was crimp-sealed, pumped down to vacuum and backfilled with Ar thrice. The degassed 2 : 1 THF : DMF mixture (6.2 mL) was added to dissolve the monomers, followed by addition of 0.6 M Na_2CO_3 solution (3.75 mL, 2.25 mmol). The solution was purged with Ar for a further 15 min before heating in a microwave at 130 °C for 15 min and then cooled. The solution was then precipitated in deionized water. The resulting precipitate was filtered over a 0.45-μm nylon membrane filter. The precipitate was then dissolved in 1 : 1 ACN : MeOH (typically about 5 mL) and added to a solution of sodium diethyldithiocarbamate in 5 mL of 1 : 1 ACN : MeOH (2.0 g, 9.2 mmol). The solution was purified by dialysis through a regenerated cellulose membrane (MWCO = 12–14 kDa), using 1 : 1 ACN : MeOH as a dialysate for 30 min. The volume ratio of the dialyzed polymer solution to the solvent bath was about 1 : 50. This step was repeated with fresh dialysate 2 more times for 30 min, and another 2 times for 1 h. The dialyzed solution was precipitated in diethyl ether and washed with water to yield poly(9,9′-bis(3′-pentaethylsulfonylimidoethyl)fluorene-2,7-diyl-1,4-phenylene-*N*-(*m*-trifluoro-methylphenyl)-amino-1,4-phenylene) sodium salt (**mTFF-C2SISC$_2$F$_5$**) as an off-white solid. ^{1}H NMR (400 MHz, DMSO-d$_6$), δ (ppm): 7.94–7.20 (m, 18H), 2.88–2.66 (m, 4H), 2.57–2.30 (m, 4H). GPC in DMF + 0.1 M LiBr: M_n = 26 kDa, M_w = 59 kDa, PDI = 2.3. Elemental analysis: C : H : N : S = 43.11% : 2.73% : 3.91% : 10.69% = 3.58 : 2.73 : 0.28 : 0.33 = 40 : 30.5 : 3.12 : 3.68 (theo 40 : 28 : 3 : 4).

Synthesis of poly(9,9′-bis(3-pentaethylsulfonylimidosulfonylpropyl)fluorene-2,7-diyl-1,4-phenylene-*N*-(*m*-trifluoromethylphenyl)imino-1,4-phenylene) sodium salt (mTFF-C3SISC$_2$F$_5$). Into a 20-mL microwave vial, equimolar portions of **diBr-FC3SISC$_2$F$_5$-TEAH** (500.00 mg, 0.44 mmol), **diEs-mTFF** (248.72 mg, 0.44 mmol) and catalytic Pd(dppf)Cl$_2$ (3 mol%) were added. The vial was crimp-sealed, pumped down to vacuum and backfilled with Ar thrice. The degassed 2 : 1 THF : DMF mixture (6.3 mL) was added to dissolve the monomers, followed by addition of 0.6 M Na_2CO_3 solution (3.75 mL, 2.25 mmol). The solution was purged with Ar for a further 15 min before heating in a microwave at 130 °C for 15 min and then cooled. The solution was precipitated in deionized water. The resulting precipitate was then filtered over a 0.45-μm nylon membrane filter. The precipitate was dissolved in 1 : 1 ACN : MeOH (typically about 5 mL) and added to a solution of sodium diethyldithiocarbamate in 5 mL of 1 : 1 ACN : MeOH (2.0 g, 9.2 mmol). The solution was purified by dialysis through a regenerated cellulose membrane (MWCO = 12–14 kDa), using 1 : 1 ACN : MeOH as a dialysate for 30 min. The volume ratio of the dialyzed polymer solution to the solvent bath was about 1 : 50. This step was repeated with fresh dialysate 2 more times for 30 min, and another 2 times for 1 h. The dialyzed solution was precipitated in diethyl ether and washed with deionized water to yield poly(9,9′-bis(3′-pentaethylsulfonylimidopropyl)fluorene-2,7-diyl-1,4-phenylene-*N*-(*m*-trifluoro-methylphenyl)-amino-1,4-phenylene) sodium salt (**mTFF-C3SISC$_2$F$_5$**) as an off-white solid. ^{1}H NMR (400 MHz, DMSO-d$_6$), δ (ppm): 7.98–7.11 (m, 18H), 2.85–2.69 (m, 4H), 2.30–2.10 (m, 4H), 1.06–0.88 (m, 4H). GPC in DMF + 0.1 M LiBr: M_n = 23 kDa, M_w = 47 kDa, PDI = 2.1. Elemental analysis: C : H : N : S = 43.32% : 3.04% : 3.77% : 10.77% = 3.61 : 3.04 : 0.27 : 0.34 = 42 : 35.3 : 3.14 : 3.95 (theo 42 : 32 : 3 : 4).

Synthesis of poly(9,9′-bis(4-pentaethylsulfonylimidosulfonylbutyl)fluorene-2,7-diyl-1,4-phenylene-*N*-(*m*-trifluoromethylphenyl)imino-1,4-phenylene) sodium salt (mTFF-C4SISC$_2$F$_5$). Into a 20-mL microwave vial, equimolar portions of **diBr-FC4SISC$_2$F$_5$-TEAH** (500.00 mg, 0.43 mmol), **diEs-mTFF** (243.07 mg, 0.43 mmol) and catalytic Pd(dppf)Cl$_2$ (3 mol%) were added. The vial was crimp-sealed, pumped down to vacuum and backfilled with Ar thrice. The degassed 2 : 1 THF : DMF mixture (6.4 mL) was added to dissolve the monomers, followed by addition of 0.6 M Na_2CO_3 solution (3.6 mL, 2.15 mmol). The solution was purged with Ar for a further 15 min before heating in a microwave at 130 °C for 15 min and then cooled. The solution was precipitated in deionized water. The resulting precipitate was then filtered over a 0.45-μm nylon membrane filter. The precipitate was dissolved in 1 : 1 ACN : MeOH (typically about 5 mL) and added to a solution of sodium diethyldithiocarbamate in 5 mL of 1 : 1 ACN : MeOH (1.9 g, 8.6 mmol). The solution was purified by dialysis through a regenerated cellulose membrane (MWCO = 12–14 kDa), using 1 : 1 ACN : MeOH as a dialysate for 30 min. The volume ratio of the dialyzed polymer solution to the solvent bath was about 1 : 50. This step was repeated with fresh dialysate 2 more times for 30 min, and another 2 times for 1 h. The dialyzed solution was precipitated in diethyl ether and washed with deionized water to yield poly(9,9′-bis(3′-pentaethylsulfonylimidobutyl)fluorene-2,7-diyl-1,4-phenylene-*N*-(*m*-trifluoro-methylphenyl)-amino-1,4-phenylene) sodium salt (**mTFF-C4SISC$_2$F$_5$**) as an off-white solid. ^{1}H NMR (400 MHz, DMSO-d$_6$), δ (ppm): 8.00–7.05 (m, 18H), 2.90–2.65 (m, 4H), 2.40–2.00 (m, 4H), 1.60–1.40 (m, 4H), 0.80–0.50 (m, 4H). GPC in DMF + 0.1 M LiBr: M_n = 14 kDa, M_w = 20 kDa, PDI = 1.4. Elemental analysis: C : H : N : S = 43.39% : 3.41% : 3.69% : 10.49% = 3.61 : 3.41 : 0.26 : 0.33 = 44 : 41.6 : 3.17 : 4.02 (theo 44 : 36 : 3 : 4).

Synthesis of poly(9,9′-bis(6-pentaethylsulfonylimidosulfonylhexyl)-fluorene-2,7-diyl-1,4-phenylene-*N*-(*m*-trifluoromethylphenyl)imino-1,4-phenylene) sodium salt (mTFF-C6SISC$_2$F$_5$). Into a 20-mL microwave vial, equimolar portions of **diBr-FC6SISC$_2$F$_5$-Na** (500.00 mg, 0.47 mmol), **diEs-mTFF** (267.00 mg, 0.47 mmol) and catalytic Pd(dppf)Cl$_2$ (3 mol%) were added. The vial was crimp-sealed, pumped down to vacuum and backfilled with Ar thrice. The degassed 2 : 1 THF : DMF mixture (6.1 mL) was added to dissolve the monomers, followed by addition of 0.6 M Na_2CO_3 solution (3.9 mL, 2.35 mmol). The solution was purged with Ar for a further 15 min before heating in a microwave at 130 °C for 15 min and then cooled. The solution was precipitated in

deionized water. The resulting precipitate was then filtered over a 0.45-μm nylon membrane filter. The precipitate was dissolved in 1 : 1 ACN : MeOH (typically about 5 mL) and added to a solution of sodium diethyldithiocarbamate in 5 mL of 1 : 1 ACN : MeOH (2.1 g, 9.4 mmol). The solution was purified by dialysis through a regenerated cellulose membrane (MWCO = 12–14 kDa), using 1 : 1 ACN : MeOH as a dialysate for 30 min. The volume ratio of the dialyzed polymer solution to the solvent bath was about 1 : 50. This step was repeated with fresh dialysate 2 more times for 30 min, and another 2 times for 1 h. The dialyzed solution was precipitated in diethyl ether and washed with deionized water to yield poly(9,9′-bis(3′-pentaethylsulfonylimidohexyl)fluorene-2,7-diyl-1,4-phenylene-*N*-(*m*-trifluoro-methylphenyl)-amino-1,4-phenylene) sodium salt (**mTFF-C6SISC$_2$F$_5$**) as an off-white solid. ^{1}H NMR (400 MHz, DMSO-d$_6$), δ (ppm): 8.21–7.00 (m, 18H), 2.89–2.73 (m, 4H), 2.30–1.95 (m, 4H), 1.56–1.38 (m, 4H), 1.21–0.95 (m, 8H), 0.74–0.40 (m, 4H). GPC in DMF + 0.1 M LiBr: M_n = 19 kDa, M_w = 30 kDa, PDI = 1.6. Elemental analysis: C : H : N : S = 46.03% : 3.79% : 3.56% : 9.74% = 3.83 : 3.79 : 0.25 : 0.30 = 48 : 47.5 : 3.13 : 3.76 (theo 48 : 44 : 3 : 4).

Doping methods

Film-doping. In a typical procedure, the mTFF-C*n*SISC$_2$F$_5$ film, where n = 2 and 6, was spin-cast from 10 mg mL^{-1} in ACN onto desired substrates and annealed at 120 °C (hotplate, 10 min) in a nitrogen glovebox. The film was contacted (10 s) with tris-(*p*-bromophenyl)aminium hexachloroantimonate (TBPASbCl$_6$) (0.4 mM) *p*-dopant in anhydrous ACN : DMC (1 : 10) in the glovebox and excess dopant spun-off to dope the film. The excess ions and salt by-products were removed by two consecutive spin-rinse steps in the same solvent mixture to give the self-compensated, hole-doped film.

Solution-doping. In a typical procedure, mTFF-C*n*SISC$_2$F$_5$, where n = 2, 3 and 4, was dissolved in anhydrous ACN to 22 mg mL^{-1}. 1 equivalent of NOSbF$_6$ (40 mM) was added and precipitated with DMC to eliminate the soluble salt by-product. The precipitated solid was re-dissolved in anhydrous ACN and precipitated with DMC once more, and finally re-dissolve in anhydrous ACN without drying in vacuum to give a solution of the self-compensated, hole-doped polymer. Self-compensated, hole-doped polymer films can then be spin-cast from the solution onto desired substrates.

Ultraviolet and X-ray photoemission spectroscopy. The films were prepared on O$_2$-plasma-cleaned Au-coated Si substrates in a N$_2$ glovebox, and transferred in N$_2$ without exposure to air into the UHV chamber load lock. UPS was performed using He I radiation (21.21 eV) in a VG ESCALab Mk-II spectrometer operated at a base pressure of 1×10^{-9} mbar. A sample bias of −5.00 V was applied to collect all the photoemission. XPS was performed using a VG ESCALab Mk-II spectrometer with MgKα X-rays (1253.6 eV) set at a magic angle of 54.9° with respect to the analyzer.

UV-Vis-NIR spectroscopy. UV-Vis-NIR spectroscopy was performed using an Ocean Optics S1024DW Deep Well spectrometer with a DH-2000 deuterium tungsten halogen light source.

Thermogravimetry. Thermogravimetry was performed on Discovery TGA 1 (TA Instruments). Powder samples were prepared by diethylether precipitation from ACN, stored in a N$_2$ glovebox overnight (pH_2O < 1 ppm) and only briefly exposed to the ambient atmosphere (<5 min; 25 °C, 65% RH) during sample loading. Samples in powder form (4–6 mg) were loaded under ambient conditions (22 °C, 65–70% RH) onto the sample pan which was then moved into the nitrogen-purged furnace under computer control. Scan parameters: isothermal hold at 35 °C for 10 min, temperature ramp at 5 °C min^{-1} to 230 °C, isothermal hold for 10 min, temperature ramp at −5 °C min^{-1} to 35 °C, all in flowing nitrogen (>99.999% purity). The samples were exposed to the ambient atmosphere for 2 h before repeating the scan.

Molecular dynamics simulations. OPLS4 calculations were performed in MacroModel (Schrödinger LLC). Five oligomer chains of SC hole-doped mTFF-C*n*SISC$_2$F$_5$ with three repeat units each were randomly placed. Aminium N$^+$ was simulated by C$^+$. Fifteen Na$^+$ cations were added for charge neutrality. The structures were annealed at 300 K for 5 ns in a background dielectric constant of 3.0, followed by energy minimization. At least 10 different seed configurations were launched to sample different ion cluster morphology.

Device fabrication. 30–43-nm thick hole-doped mTFF-C*n*SISC$_2$F$_5$ films were deposited onto O$_2$-plasma cleaned indium tin oxide (ITO) substrates in a N$_2$ glovebox to form hole-injection layers (HILs). The poly(9,9-bis(4-octylphenyl)fluorene-2,7-diyl) (PFOP) solution (10 mg mL^{-1}) was prepared in toluene and spin-cast over the HILs to form 90-nm-thick films. The 120-nm-thick Al film was then thermally evaporated through a shadow mask at a base pressure of 10^{-7} Torr to give eight 4.3 mm^2 cathode pixels on each substrate. For n = 2, the film thickness is 38 nm; for n = 3, it is 33 nm; for n = 4, it is 43 nm; for n = 2 (film doped), the film thickness is 37 nm; and for n = 6 (film doped), it is 32 nm.

Electroabsorption spectroscopy. Electroabsorption (EA) spectroscopy measurements of the diodes were performed at 30 K in a closed-cycle helium cryostat (Janis APD HC-2). The pressure inside the chamber was maintained at 10^{-5} Torr. A sinusoidal drive voltage superposed on the selected dc bias was injected into the diode. Monochromatic light was incident through the glass substrate at 45°, and its reflection from the cathode was then collected by mirror optics onto a photodiode. The voltage output was demodulated by a lock-in amplifier phase locked to the ac to give the change in absorbance for a range of wavelength.

Author contributions

L. L. C. directed material development and characterization. Q. M. K. conducted the experiments. C. G. T. conducted the electroabsorption measurement. R. Q. P. performed the OPLS4 calculations. Q. M. K., K. C. B., Y. W. and Q. J. S. contributed to material development. P. H. K. H. provided advice. Q. M. K., R. Q. P. and L. L. C. wrote the manuscript. All authors discussed the experiments and results.

Data availability

The data that support the findings of this study are all available in the article.

Conflicts of interest

There is no conflict to declare.

Acknowledgements

This research is partially supported by the National Research Foundation, Prime Minister's Office, Singapore, under its Competitive Research Programme (CRP Award No. NRF-CRP24-2020-0006: A-0008375-00-00, A-0008375-01-00).

References

1 C. G. Tang, M. C. Ang, K. K. Choo, V. Keerthi, J. K. Tan, M. N. Syafiqah, T. Kugler, J. H. Burroughes, R. Q. Png, L. L. Chua and P. K. H. Ho, Doped polymer semiconductors with ultrahigh and ultralow work functions for ohmic contacts, *Nature*, 2016, **539**, 536–540.

2 C. G. Tang, M. N. Syafiqah, Q. M. Koh, C. Zhao, J. Zaini, Q. J. Seah, M. J. Cass, M. J. Humphries, I. Grizzi, J. H. Burroughes, R. Q. Png, L. L. Chua and P. K. H. Ho, Multivalent anions as universal latent electron donors, *Nature*, 2019, **573**, 519–525.

3 S. A. Chen and M. Y. Hua, Structure and doping level of the self-acid-doped conjugated conducting polymers: poly[*n*-(3'-thienyl)alkanesulfonic acids], *Macromolecules*, 1993, **26**, 7108–7110.

4 H. S. O. Chan, P. K. H. Ho, S. C. Ng, B. T. G. Tan and K. L. Tan, A new water-soluble, self-doping conducting polyaniline from poly(*o*-aminobenzylphosphonic acid) and its sodium salts: synthesis and characterization, *J. Am. Chem. Soc.*, 1995, **117**, 8517–8523.

5 T. H. Reilly III, A. W. Hains, H.-Y. Chen and B. A. Gregg, A self-doping, O2-stable, n-type interfacial layer for organic electronics, *Adv. Energy Mater.*, 2012, **2**, 455–460.

6 C. K. Mai, H. Zhou, Y. Zhang, Z. B. Henson, T. Q. Nguyen, A. J. Heeger and G. C. Bazan, Facile doping of anionic narrow-band-gap conjugated polyelectrolytes during dialysis, *Angew. Chem., Int. Ed.*, 2013, **52**, 12874–12878.

7 S. Watanabe, R. Hakamatani, K. Yaegashi, Y. Yamashita, H. Nozawa, M. Sasaki, S. Kumagai, T. Okamoto, C. G. Tang, L. L. Chua, P. K. H. Ho and J. Takeya, Surface doping of organic single-crystal semiconductors to produce strain-sensitive conductive nanosheets, *Adv. Sci.*, 2021, **8**, 2002065.

8 C. Zhao, C. G. Tang, Z. L. Seah, Q. M. Koh, L. L. Chua, R. Q. Png and P. K. H. Ho, Improving organic photovoltaic cells by forcing electrode work function well beyond onset of Ohmic transition, *Nat. Commun.*, 2021, **12**, 2250.

9 K. Philipps, Y. Ie, B. van der Zee, R. Q. Png, P. K. H. Ho, L. L. Chua, E. del Pino Rosendo, C. Ramanan, G. J. A. H. Wetzelaer, P. W. M. Blom and J. J. Michels, Role of linker functionality in polymers exhibiting main-chain thermally activated delayed fluorescence, *Adv. Sci.*, 2022, **9**, 2200056.

10 X. Tan, D. Dou, L. L. Chua, R. Q. Png, D. G. Congrave, H. Bronstein, M. Baumgarten, Y. Li, P. W. M. Blom and G.-J. A. H. Wetzelaer, Inverted device architecture for high efficiency single-layer organic light-emitting diodes with imbalanced charge transport, *Nat. Commun.*, 2024, **15**, 4107.

11 B. vander Zee, S. Paulus, R. Q. Png, P. K. H. Ho, L. L. Chua, G. J. A. H. Wetzelaer and P. W. M. Blom, Role of singlet and triplet excitons on the electrical stability of polymer light-emitting diodes, *Adv. Electron. Mater.*, 2020, **6**, 2000367.

12 A. G. Ricciardulli, B. van der Zee, K. Philipps, G. A. H. Wetzelaer, R. Q. Png, P. K. H. Ho, L. L. Chua and P. W. M. Blom, Polymer–perovskite blend light-emitting diodes using a self-compensated heavily doped polymeric anode, *APL Mater.*, 2020, **8**, 021101.

13 L. X. Wang, C. G. Tang, Z. S. Tan, H. Y. Phua, J. Chen, W. Lei, R. Q. Png, L. L. Chua and P. K. H. Ho, Double-type-I charge-injection heterostructure for quantum-dot light-emitting diodes, *Mater. Horiz.*, 2022, **9**, 2147–2159.

14 R. Q. Png, M. C. Ang, M. H. Teo, K. K. Choo, C. G. Tang, D. Belaineh, L. L. Chua and P. K. H. Ho, Madelung and Hubbard interactions in polaron band model of doped organic semiconductors, *Nat. Commun.*, 2016, **7**, 11948.

15 M. C. Y. Ang, Q. M. Koh, C. G. Tang, Q. J. Seah, Y. Wang, M. Callsen, Y. P. Feng, R. Q. Png and L. L. Chua, Spectator cation size effect on the work function and stability of self-compensated hole-doped polymers, *J. Mater. Chem. C*, 2020, **8**, 124–131.

16 M. C. Y. Ang, C. G. Tang, Q. M. Koh, C. Zhao, Q. J. Seah, Y. Wang, M. Callsen, Y. P. Feng, R. Q. Png and L. L. Chua, Bulk ion-clustering and surface ion-layering effects on work function of self-compensated charged-doped polymer semiconductors, *Mater. Horiz.*, 2020, **7**, 1073–1082.

17 Q. M. Koh, N. S. Mazlan, Q. J. Seah, J. C. Yang, Y. J. Chen, R. Q. Png, P. K. H. Ho and L. L. Chua, Effects of planarization of the triphenylamine unit on the electronic and transport properties of triarylamine–fluorene copolymers in both doped and undoped forms, *ACS Appl. Mater. Interfaces*, 2024, **16**, 39708–39716.

18 Q. M. Koh, C. G. Tang, M. C. Y. Ang, K. K. Choo, Q. J. Seah, R. Q. Png, L. L. Chua and P. K. H. Ho, Overcoming the water oxidative limit for ultra-high-workfunction hole-doped polymers, *Nat. Commun.*, 2021, **12**, 3345.

19 C. G. Tang, M. Nur Syafiqah, Q. M. Koh, M. C. Y. Ang, K. K. Choo, M. M. Sun, M. Callsen, Y. P. Feng, L. L. Chua, R. Q. Png and P. K. H. Ho, Water binding and hygroscopicity in π-conjugated polyelectrolytes, *Nat. Commun.*, 2023, **14**, 3978.

20 F. M. Koch and R. Peters, Catalytic enantio- and diastereoselective formation of β-Sultones: ring-strained precursors for enantioenriched β-hydroxysulfonyl derivatives, *Angew. Chem., Int. Ed.*, 2007, **46**, 2685–2689.

21 J. C. Yan, X. Cheng, Q. L. Zhou and J. Pei, Chiral polyfluorene derivatives: Synthesis, chiroptical properties, and investigation of

the structure–property relationships, *Macromolecules*, 2007, **40**, 832–839.

22 V. V. Sureshbabu, T. M. Vishwanatha and B. Vasantha, A simple synthesis of Nβ-Fmoc/Z-amino alkyl thiols and their use in the synthesis of Nβ-Fmoc/Z-amino alkyl sulfonic acids, *Synlett*, 2010, 1037–1042.

23 W. L. Seah, C. G. Tang, R. Q. Png, V. Keerthi, C. Zhao, H. Guo, J. G. Yang, M. Zhou, P. K. H. Ho and L. L. Chua, Interface doping for ohmic organic semiconductor contacts using self-aligned polyelectrolyte counterion monolayer, *Adv. Funct. Mater.*, 2017, **27**, 1606291.

24 C. Lu, C. Wu, D. Ghoreishi, W. Chen, L. Wang, W. Damm, G. A. Ross, M. K. Dahlgren, E. Russell, C. D. Von Bargen, R. Abel, R. A. Friesner and E. D. Harder, OPLS4: Improving force field accuracy on challenging regimes of chemical space, *J. Chem. Theory Comput.*, 2021, **17**, 4291–4300.

25 P. J. Chia, S. Sivaramakrishnan, M. Zhou, R. Q. Png, L. L. Chua, R. H. Friend and P. K. H. Ho, Direct evidence for the role of the Madelung potential in determining the work function of doped organic semiconductors, *Phys. Rev. Lett.*, 2009, **102**, 096602.

26 I. H. Campbell, M. D. Joswick and I. D. Parker, Direct measurement of the internal electric field distribution in a multilayer organic light-emitting diode, *Appl. Phys. Lett.*, 1995, **67**, 3171–3173.

27 V. Bodrozic, T. M. Brown, S. Mian, D. Caruana, M. Roberts, N. Phillips, J. J. Halls, I. Grizzi, J. H. Burroughes and F. Cacialli, The built-In potential in blue polyfluorene-based light-emitting diodes, *Adv. Mater.*, 2008, **20**, 2410–2415.

28 M. Zhou, L. L. Chua, R. Q. Png, C. K. Yong, S. Sivaramakrishnan, P. J. Chia, A. T. S. Wee, R. H. Friend and P. K. H. Ho, The role of delta-doped interfaces for Ohmic contacts to organic semiconductors, *Phys. Rev. Lett.*, 2009, **103**, 036601–036604.

29 M. Zhou, R. Q. Png, S. H. Khong, S. Sivaramakrishnan, L. H. Zhao, L. L. Chua, R. H. Friend and P. K. H. Ho, Effective work functions for the evaporated metal/organic semiconductor contacts from in-situ diode flatband potential measurements, *Appl. Phys. Lett.*, 2012, **101**, 013501.

30 Q. M. Koh, Q. J. Seah, J. C. Yang, N. S. Mazlan, Q. E. Hoh, Z. L. Seah, R. Q. Png, P. K. H. Ho and L. L. Chua, Evidence for morphology control by polyelectrolyte templating in PEDT:PSSH, *Adv. Funct. Mater.*, 2024, 2407493.

31 C. V. Hoven, A. Garcia, G. C. Bazan and T. Q. Nguyen, Recent applications of conjugated polyelectrolytes in optoelectronic devices, *Adv. Mater.*, 2008, **20**, 3793–3810.

32 F. Huang, H. Wu and Y. Cao, Water/alcohol soluble conjugated polymers as highly efficient electron transporting/injection layer in optoelectronic devices, *Chem. Soc. Rev.*, 2010, **39**, 2500–2521.

33 J. H. Lee, B. H. Lee, S. Y. Jeong, S. B. Park, G. Kim, S. H. Lee and K. Lee, Radical cation–anion coupling-induced work function tunability in anionic conjugated polyelectrolytes, *Adv. Energy Mater.*, 2015, **5**, 1501292.

34 D. Belaineh, J. K. Tan, R. Q. Png, P. F. Dee, Y. M. Lee, B. N. N. Thi, N. S. Ridzuan and P. K. H. Ho, Perfluorinated ionomer-modified hole-injection layers: ultrahigh workfunction but nonohmic contacts, *Adv. Funct. Mater.*, 2015, **25**, 5504–5511.